Indosinian high-strain deformation for the Yunkaidashan tectonic belt, south China: Kinematics and $^{40}Ar/^{39}Ar$ geochronological constraints

Yuejun Wang,[1,2] Weiming Fan,[1] Peter A. Cawood,[3] Shaocheng Ji,[1] Touping Peng,[1] and Xinyue Chen[1]

Received 4 January 2007; revised 25 August 2007; accepted 5 September 2007; published 14 December 2007.

[1] Structural and $^{40}Ar/^{39}Ar$ data from the Yunkaidashan Belt document kinematic and tectonothermal characteristics of early Mesozoic Indosinian orogenesis in the southern part of the South China Block. The Yunkaidashan Belt is tectonically divided from east to west into the Wuchuang-Sihui shear zone, Xinyi-Gaozhou block, and the Fengshan-Qinxi shear zone. Indosinian structural elements ascribed to the Indosinian orogeny include D_2 and D_3 deformation. The early D_2 phase is characterized by folding and thrusting with associated foliation and lineation development, related to NW-SE transpression under amphibolite- to greenschist-facies conditions. This event is heterogeneously overprinted by D_3 deformation characterized by a gentle-dipping S_3 foliation, subhorizontally to shallowly plunging L_3 lineation, some reactived-D_2 folds and low-angle normal faults. The D_3 fabrics suggest a sinistral transtensional regime under greenschist-facies metamorphism. The timing of the D_2 and D_3 events have been constrained to the early to middle Triassic (~248–220 Ma) and late Triassic (~220–200 Ma) respectively on the basis of $^{40}Ar/^{39}Ar$ geochronology and regional geological relations. The change from oblique thrusting (D_2) to sinistral transtension (D_3) may reflect oblique convergence and crustal thickening followed by relaxation of the overthickened crust. In combination with the regional relations from Xuefengshan to Yunkaidashan and on to Wuyishan, the early phase of the Indosinian orogeny constituted a large-scale positive flower structure and is related to the intracontinental convergence during the assembly of Pangea in which the less competent South China Orogen was squeezed between the more competent North China and Indosinian Blocks. **Citation:** Wang, Y., W. Fan, P. A. Cawood, S. Ji, T. Peng, and X. Chen (2007), Indosinian high-strain deformation for the Yunkaidashan tectonic belt, south China: Kinematics and $^{40}Ar/^{39}Ar$ geochronological constraints, *Tectonics*, *26*, TC6008, doi:10.1029/2007TC002099.

1. Introduction

[2] The early Mesozoic Indosinian orogeny created the tectonic framework of eastern China (Figure 1a) through its accretion to Eurasia [e.g., *Huang et al.*, 1987; *Ren*, 1991]. This orogenic pulse was originally inferred from the presence of angular unconformities within Triassic strata but is increasingly recognized in studies of structural fabrics and granitic magmatism [e.g., *Deprat*, 1914; *Fromaget*, 1932; *Holloway*, 1982; *Hsü et al.*, 1990; *Li et al.*, 2006; *Chen*, 1999; *Y. J. Wang et al.*, 2005a, 2005b, 2007a, and references therein]. In the South China Block, the Indosinian orogeny is marked by a pre-upper Triassic unconformity and widespread magma emplacement [*Bureau of Geology and Mineral Resources of Jiangxi Province*, 1984; *Hunan Bureau of Geology and Mineral Resources*, 1988; *Xu et al.*, 2003; *Deng et al.*, 2004; *Y. J. Wang et al.*, 2005a, 2005b, 2007a, and reference therein], however, the structural signatures and thermochronology of the orogeny are still poorly documented. In particular, there is a lack of consensus on the tectonic setting during orogenesis with some researchers proposing an overall compressive regime related to oblique subduction of the paleo-Pacific plate [e.g., *Holloway*, 1982; *Hsü et al.*, 1990; *Faure et al.*, 1996; *Li*, 1998; *Zhou and Li*, 2000; *Q. Wang et al.*, 2005; *Li et al.*, 2006; *Li and Li*, 2007], whereas others have argued for intracontinental collisional setting involving a rift weak zone [e.g., *Y. J. Wang et al.*, 2005b, 2007a; *Chen*, 1999].

[3] In this paper, we outline structural and $^{40}Ar/^{39}Ar$ geochronological data from the Yunkaidashan belt, an important strain belt with abundant ductile shearing and thrust-and-fold signatures that lies within the southern part of the South China Block (see Figure 1b) to document the kinematic and tectonothermal character of the Indosinian orogeny. This information is integrated with available data from the Xuefengshan, northern Wuyishan and Wugongshan zones in the northern part of the block [*Y. J. Wang et al.*, 2005b; *Yan et al.*, 2003; *Chen*, 1999; *Faure et al.*, 1996] to better constrain tectonic setting during orogenesis.

[1]Key Laboratory of Isotope Geochronology and Geochemistry, Guangzhou Institute of Geochemistry, Chinese Academy of Sciences, Guangzhou, China.
[2]Department of Geology, Northwest University, Xi'an, China.
[3]Tectonics Special Research Centre, University of Western Australia, Crawley, Western Australia, Australia.

0278-7407/07/2007TC002099$12.00

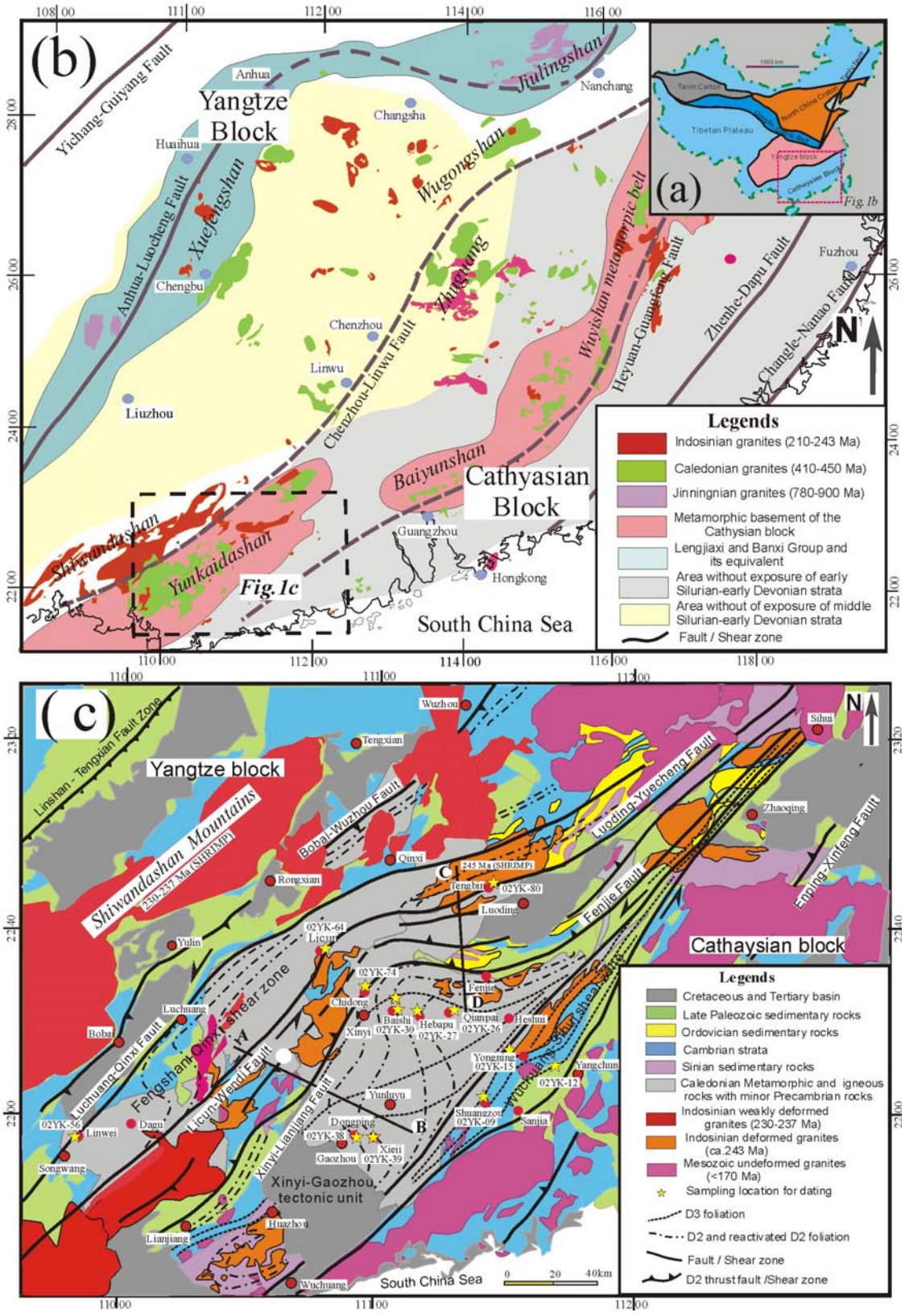
(b)
Yangtze Block
Cathyasian Block
Yichang-Guiyang Fault
Anhua-Luocheng Fault
Xuefengshan
Jiulingshan
Wugongshan
Zhuguang
Chenzhou-Linwu Fault
Wuyishan metamorphic belt
Heyuan-Guangfeng Fault
Zhenhe-Dapu Fault
Changle-Nanao Fault
Baiyunshan
Shiwandashan
Yunkaidashan
Fig.1c
South China Sea
Anhua
Nanchang
Changsha
Huaihua
Chengbu
Chenzhou
Linwu
Liuzhou
Fuzhou
Guangzhou
Hongkong
Tarim Carton
North China Craton
Tibetan Plateau
Yangtze block
Cathaysian Block
Fig.1b
(a)
N
Legends
Indosinian granites (210-243 Ma)
Caledonian granites (410-450 Ma)
Jinningnian granites (780-900 Ma)
Metamorphic basement of the Cathysian block
Lengjiaxi and Banxi Group and its equivalent
Area without exposure of early Silurian-early Devonian strata
Area without of exposure of middle Silurian-early Devonian strata
Fault / Shear zone
(c)
Yangtze block
Cathaysian block
Shiwandashan Mountains
230-237 Ma (SHRIMP)
Linshan - Tengxian Fault Zone
Bobai-Wuzhou Fault
Luoding-Yuecheng Fault
Fenjie Fault
Enping-Xinfeng Fault
Fengshan-Qinxi shear zone
Luchuang-Qinxi Fault
Licun-Wendi Fault
Xinyi-Lianjiang Fault
Xinyi-Gaozhou tectonic unit
Wuzhou
Tengxian
Silui
Zhaoqing
Qinxi
Rongxian
Yulin
Luchuang
Bobai
Linwei
Dagu
Songwang
Huazhou
Lianjiang
Wuchuang
Chidong
Baishi
Xinyi
Hebapu
Qianpai
Heshui
Fenjie
Luoding
Licun
Tengbu
Yongning
Yangchun
Yunluyu
Shuangzou
Sanjia
Dongning
Gaozhou
Xieji
02YK-56
02YK-64
02YK-74
02YK-30
02YK-27
02YK-26
02YK-80
02YK-15
02YK-12
02YK-09
02YK-38
02YK-39
245 Ma (SHRIMP)
A
B
C
D
South China Sea
0 20 40km
Legends
Cretaceous and Tertiary basin
Late Paleozoic sedimentary rocks
Ordovician sedimentary rocks
Cambrian strata
Sinian sedimentary rocks
Caledonian Metamorphic and igneous rocks with minor Precambrian rocks
Indosinian weakly deformed granites (230-237 Ma)
Indosinian deformed granites (ca.243 Ma)
Mesozoic undeformed granites (<170 Ma)
Sampling location for dating
D3 foliation
D2 and reactivated D2 foliation
Fault / Shear zone
D2 thrust fault /Shear zone

Figure 1

[4] Our analysis indicates that the early phase of the Indosinian orogeny in South China constituted a large-scale positive flower structure involving top-to-SE and -NW thrusting with a sinistral strike-slip component. This took place during intracontinental convergence associated with the assembly of Pangea in which the less competent South China Orogen was squeezed between the more competent North China and Indosinian Blocks.

2. Geological Background

[5] The NE/ENE-trending Yunkaidashan Belt lies along the southern segment of the boundary between the Yangtze and Cathyasian blocks of the South China Block [*Chen and Jahn*, 1998]. The belt is up to 150 km wide and over 300 km long and extends northeastward into the Baiyunshan and Wuyishan metamorphic belts (Figure 1b). It is bounded to the west by the Late Permian to Middle Triassic Shiwandashan foreland basin [*Liang et al.*, 2004; *Liang and Li*, 2005], which contains extensive early Indosinian peraluminous granites [*Deng et al.*, 2004]. To the east relationships are obscured by younger Mesozoic and Cenozoic extensional basins [*Bureau of Geology and Mineral Resources of Guangxi Zhuang Autonomous Region*, 1985; *Bureau of Geology and Mineral Resources of Guangdong Province*, 1988].

[6] The Yunkaidashan Belt is traditionally considered to be composed of Precambrian metamorphic basement (e.g., Yunkai Group), Paleozoic and Mesozoic sedimentary cover, and voluminous mid-Paleozoic foliated granites [e.g., *Bureau of Geology and Mineral Resources of Guangdong Province*, 1988; *Bureau of Geology and Mineral Resources of Guangxi Zhuang Autonomous Region*, 1985; *Peng et al.*, 1996]. The Precambrian rocks were believed to be the main rock type in the Yunkaidashan belt and were considered to consist of the ''lower basement'' with high-grade metamorphic rocks and ''upper basement'' with greenschist-facies sedimentary rocks [e.g., *Bureau of Geology and Mineral Resources of Guangdong Province*, 1988; *Peng et al.*, 1996; *S. B. Peng et al.*, 2006]. However, LA-ICPMS and SHRIMP zircon U-Pb dating from the ''lower basement'' orthogneiss have given Paleozoic Caledonian ages of 467–413 Ma [*Wang et al.*, 1999; *S. B. Peng et al.*, 2006; *Wang et al.*, 2007b; Y. S. Wang personal communication, 2006]. Similarly, U-Pb dating of detrital zircons from the metasedimentary rocks (paragneiss and schist) within parts of the ''upper basement'' have yielded ages as young as ~423 Ma [*Wang et al.*, 2007b; *Xu et al.*, 2005; Y. S. Wang personal communication, 2006] suggesting that the extent of Precambrian rocks may be less than previously estimated and that most of the sedimentary successions accumulated in the early to mid Paleozoic [*Wang et al.*, 2007b].

[7] At the margin of the Yunkaidashan Belt (e.g., Yangchun, Luoding and Beiliu), there are greenschist-facies upper Devonian shales, sandstones and conglomerates, Carboniferous and Permian limestones and mudstone. These rocks are unconformable on Caledonian metaigneous rocks but the contact is usually reworked by faulting or ductile shearing [*Bureau of Geology and Mineral Resources of Guangxi Zhuang Autonomous Region*, 1985; *Bureau of Geology and Mineral Resources of Guangdong Province*, 1988; *Peng et al.*, 1996]. These folded upper Paleozoic sediments are in turn uncomfortably overlain by upper Triassic to lower Jurassic sandstone and conglomerate. Cretaceous sediments, which mainly occurred in the Luoding and Huazhou basins, are characterized by red beds that lie uncomfortably on pre-Cretaceous rocks.

[8] Early to mid Paleozoic granites (467–413 Ma [*Wang et al.*, 1999, 2007b; *S. B. Peng et al.*, 2006] are extensively exposed across the Yunkaidashan Belt (e.g., Huaixiang-Baishi-Qianpai and Heshui-Sihe areas [*Wang et al.*, 2007b]. Early Indosinian peraluminous granites (243–230 Ma, e.g., Napeng, Shiwandashan and Tangpeng), lying largely to the west of the Xinyang-Liangjiang and Fenjie faults (Figure 1c), are variously foliated and mylonitized [e.g., *Peng et al.*, 1996; *Deng et al.*, 2004]. Late Indosinian peraluminous granitic plutons (220–205 Ma [*B. X. Peng et al.*, 2006]) are undeformed (e.g., Tengbin) and only outcrop to the west of Luoding-Yuecheng fault. Undeformed Yanshanian (170–120 Ma) igneous rocks are poorly exposed in the interior of the belt, but are widespread to the east [e.g., *Bureau of Geology and Mineral Resources of Guangdong Province*, 1988; *Cai et al.*, 2001].

3. Main Tectonic Subdivisions

[9] Our mapping, integrated with previous work [*Bureau of Geology and Mineral Resources of Guangxi Zhuang Autonomous Region*, 1985; *Bureau of Geology and Mineral Resources of Guangdong Province*, 1988; *Peng et al.*, 1996], enables division of the Yunkaidashan Belt into three tectonic units, which from east to west are: the Wuchuang-Sihui shear zone, Xinyi-Gaozhou tectonic unit and the Fengshan-Qinxi shear zone (Figure 1c).

3.1. Wuchuang-Sihui Shear Zone

[10] The Wuchuang-Sihui shear zone is a NE-trending, 10–30 km wide and more than 100 km long zone that links with the Heyuan-Guangfeng fault to the north (Figures 1

Figure 1. (a) Sketchy map of tectonic frame in China showing the major blocks. (b) Simplified geological map of the South China Block showing the major faults and important tectonic zones/massifs (e.g., Xuefengshan, Jiulingshan, Wuyishan, Wugongshan) (after *Chen* [1999] and *Wang et al.* [2007a, 2007b]). (c) Geological map of the Yunkaidashan Belt revised and reinterpreted from the geological map of Guangdong and Guangxi Provinces [*Bureau of Geology and Mineral Resources of Guangdong Province*, 1988; *Bureau of Geology and Mineral Resources of Guangxi Zhuang Autonomous Region*, 1985]. Three subdivisions (Wuchuang-Sihui shear zone, Xinyi-Gaozhou tectonic unit and Fengshan-Qinxi shear zone) are also shown. Sections A-B and C-D are shown in Figure 5.

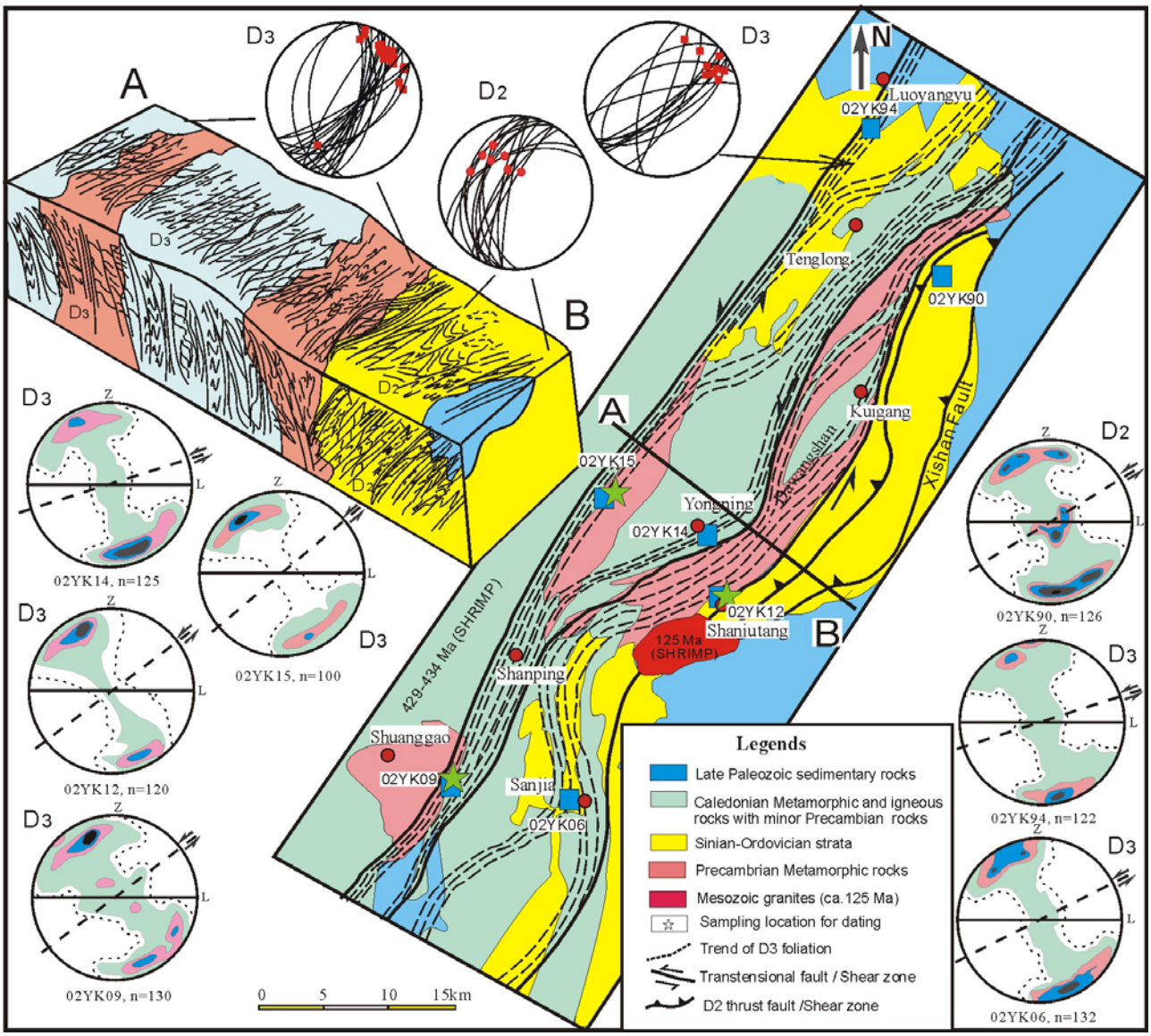

Figure 2. Geological map and cross section (A-B) across the Wuchuang-Sihui shear zone. Stereoplots (lower hemisphere, equal area) present the dominant orientation of lineation and foliation of D_2 and D_3 phases. Quartz c-axis orientation projections (lower hemisphere, equal area) are shown for the mylonitic rocks associated with D_2 (02YK-90) and D_3 (02YK-06, −09, −12, −14, −15, and −94) deformation, respectively. L and Z represent the directions of the maximum elongation and shortening, respectively. Contour intervals are 1%, 4%, 7%, and 10%.

and 2). It developed along the eastern margin of the Yunkaidashan Belt [*Bureau of Geology and Mineral Resources of Guangdong Province*, 1988]. The shear zone consists of a series of ductile high-strain zones that are up to kilometer scale in width and less than 100 km in length (e.g., Dawangshan and Luoyangyu-Shanping zones) and brittle-ductile faults (e.g., Xishan fault). These high-strain zones have an overall NE trend with a moderate to steep dips, and constitute a heterogeneous shear network (Figure 2). The Wuchuang-Sihui shear zone separates upper Paleozoic limestone and clastic rocks to the east from metamorphic basement to the west. Field observations suggest that Caledonian granite and the Proterozoic-Paleozoic metamorphic rocks in the shear zone are commonly foliated and mylonitized, and form a series of map-view shear lenses (Figure 2). High greenschist- to amphibolite-facies metamorphism with sillimanite- and cordierite-bearing mineral assemblages dominates in the shear zone.

3.2. Xinyi-Gaozhou Tectonic Unit

[11] The Xinyi-Gaozhou block has an overall NE-trend and is bounded by the Wuchuang-Sihui and Fengshan-Qinxi shear zones (Figure 1c). It comprises mainly Precambrian-Upper Paleozoic paragneiss, schist and shale, with

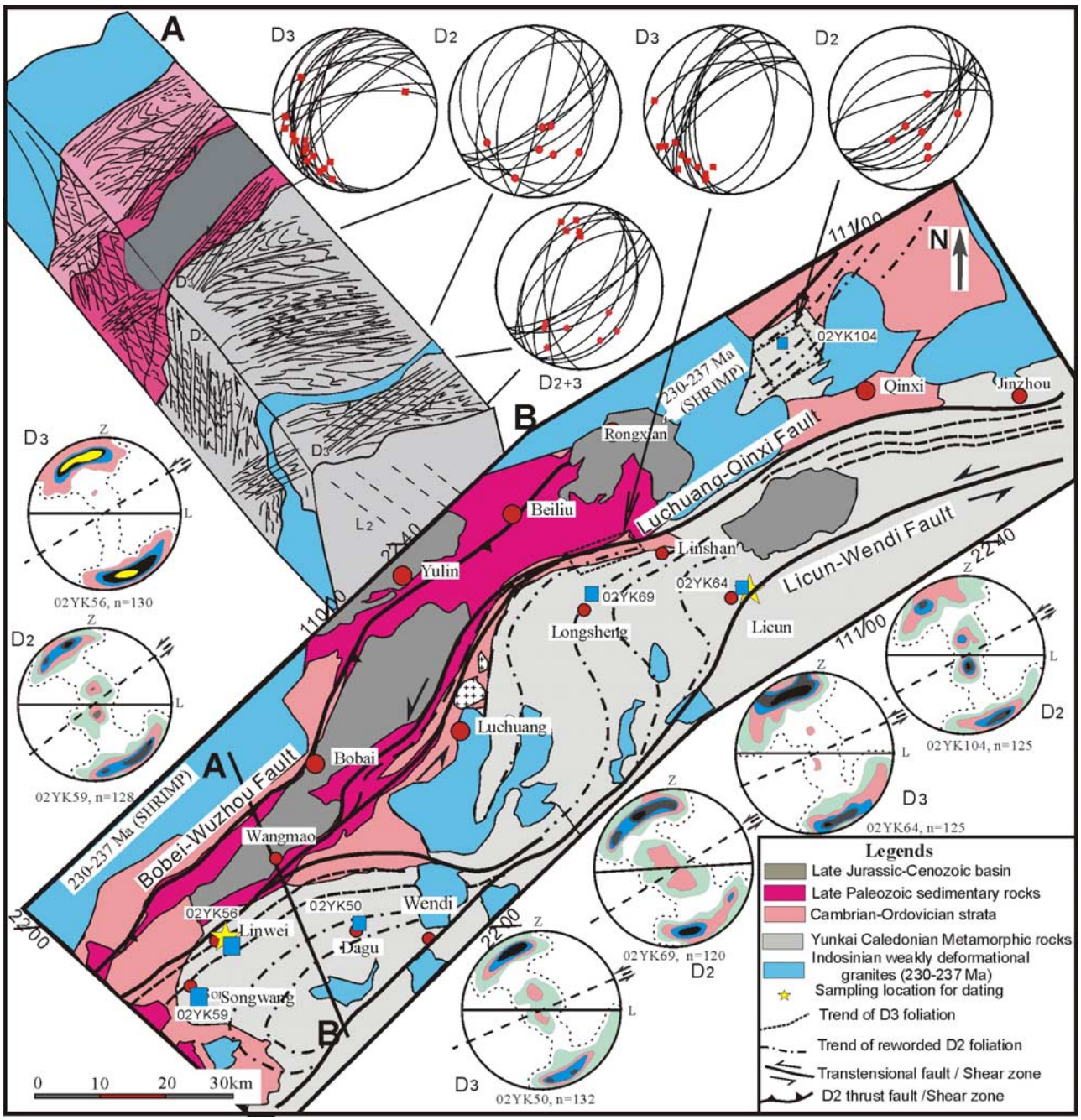

Figure 3. Geological map and cross section (A-B) across the Fengshan-Qinxi shear zone. Stereoplots (lower hemisphere, equal area) show the dominant orientation of lineation and foliation of D_2 and D_3 phases. Quartz c-axis orientation projections (lower hemisphere, equal area) are documented for the mylonitic rocks associated with D_2 (02YK −50, −59, −69, and −104) and D_3 (02YK-56 and −64) deformation, respectively. L and Z represent the directions of the maximum elongation and shortening, respectively. Contour intervals are 1%, 4%, 7%, and 10%.

weakly deformed Indosinian granites to the west of the Xinyi-Liangjiang and Fenjie faults whereas Caledonian migmatite, foliated granitoids and orthogneisses, and Paleozoic schist are better developed to the east of the faults. In the core of the unit (e.g., Xieji-Yunluyu areas), plagioclase amphibolites occur as structural lenses and veins in the orthogenesis, and granulite xenoliths occur in the foliated charnockites [e.g., *Zhou et al.*, 1994; *Chen and Zhuang*, 1994]. In the central unit, the basement underwent the amphibolite-facies metamorphism. However, toward the eastern and western margins of the unit, only a greenschist-facies metamorphism was experienced [*Zhong et al.*, 1989]. Thrust-and-fold struc-

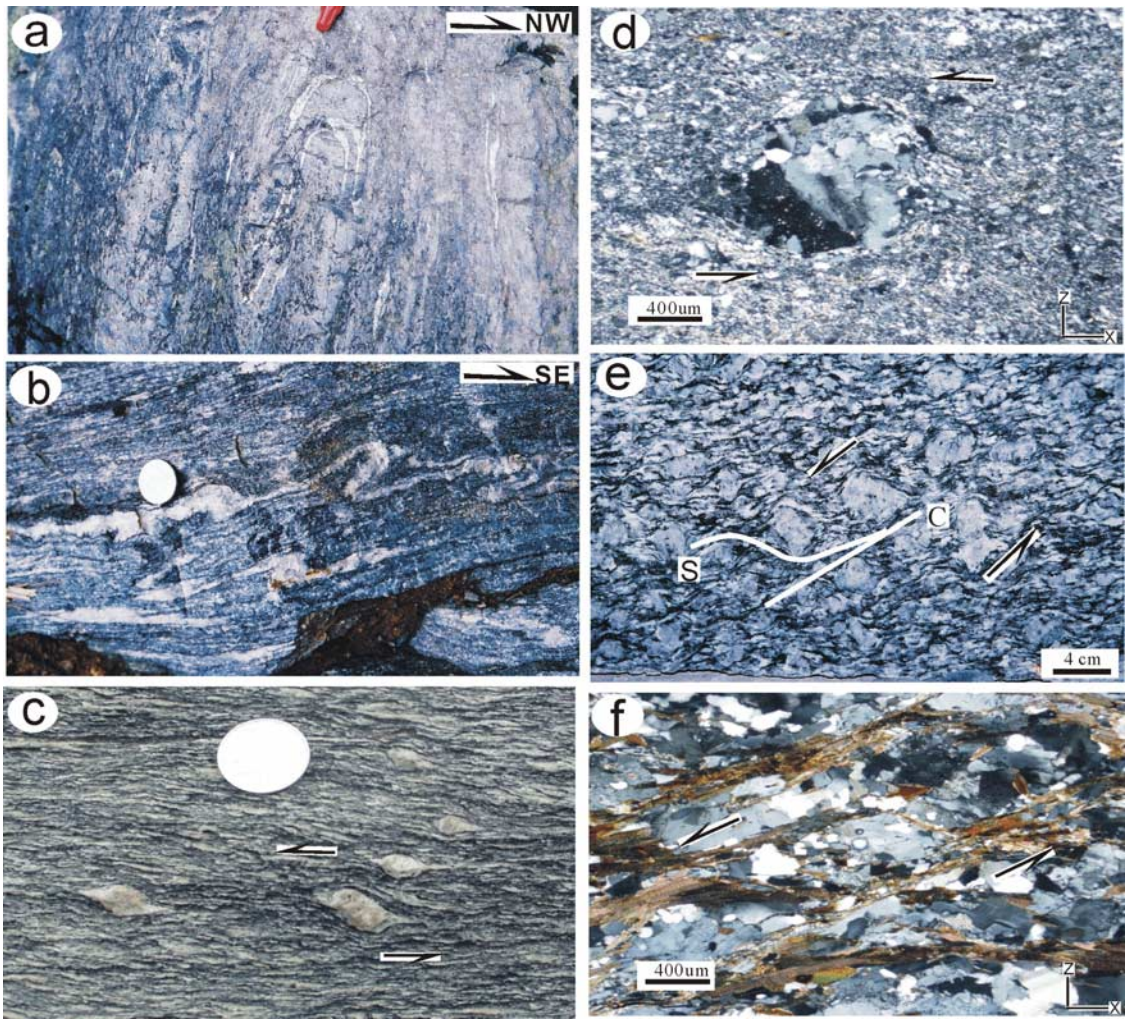

Figure 4. Photos showing D_2 structural fabrics in the Yunkaidashan tectonic Belt. (a) Inclined tight folds in foliated granites (Qianpai, Xinyi). (b) Overturned folds with an asymmetrical Z-shape geometry (Xieji, Gaozhou). (c, d) Asymmetric porphyroblasts with recrystallized tails in the outcrop and microscope, respectively (Baishi, Xinyi). (e, f) S-C fabrics in the outcrop and microscope, respectively (Hebapu, Xinyi).

tures with kilometer-scale steep to recumbent anticlines, thrust sheets and compound folds dominate in the unit and are often reactivated by a late greenschist-facies deformation event.

3.3. Fengshan-Qinxi Shear Zone

[12] The NE-trending Fengshan-Qinxi shear zone lies along the western margin of the Yunkaidashan Belt. It extends southward to Beibu Bay and northward to the Qingxi-Panlong areas to merge with the ENE-trending Luoding-Yuecheng shear zone (Figures 1c and 3). It is bounded by the Luchuan-Qinxi and Licun-Wendi high-strain zones (Figure 3), and is characterized by a series of high-strain zones ranging from 200–5000 m wide and over 100 km in length. These high-strain zones are mainly developed within the Caledonian foliated granites and Paleozoic metamorphic rocks or along their unconformable contact with younger Paleozoic strata. The Indosinian granitic plutons in the zone are similar to the cordierite-bearing peraluminous granites of the Shiwandashan Mountains to the west (237–230 Ma [*Deng et al.*, 2004]). The mylonitic rocks in this zone commonly have mineral assemblages with sillimanite ± cordierite in the schist and paragenesis, and quartz + plagioclase + biotite ± chlorite in the orthogneiss.

4. Deformational Phases

[13] Structural overprinting relationships indicate that at least four phases of deformation can be identified in the Yunkaidashan Belt. The earliest deformation (D_1, possibly related to the early Caledonian tectonothermal event) is characterized by the development of a shallow-dipping S_1 migmatitic foliation defined by compositional layering in

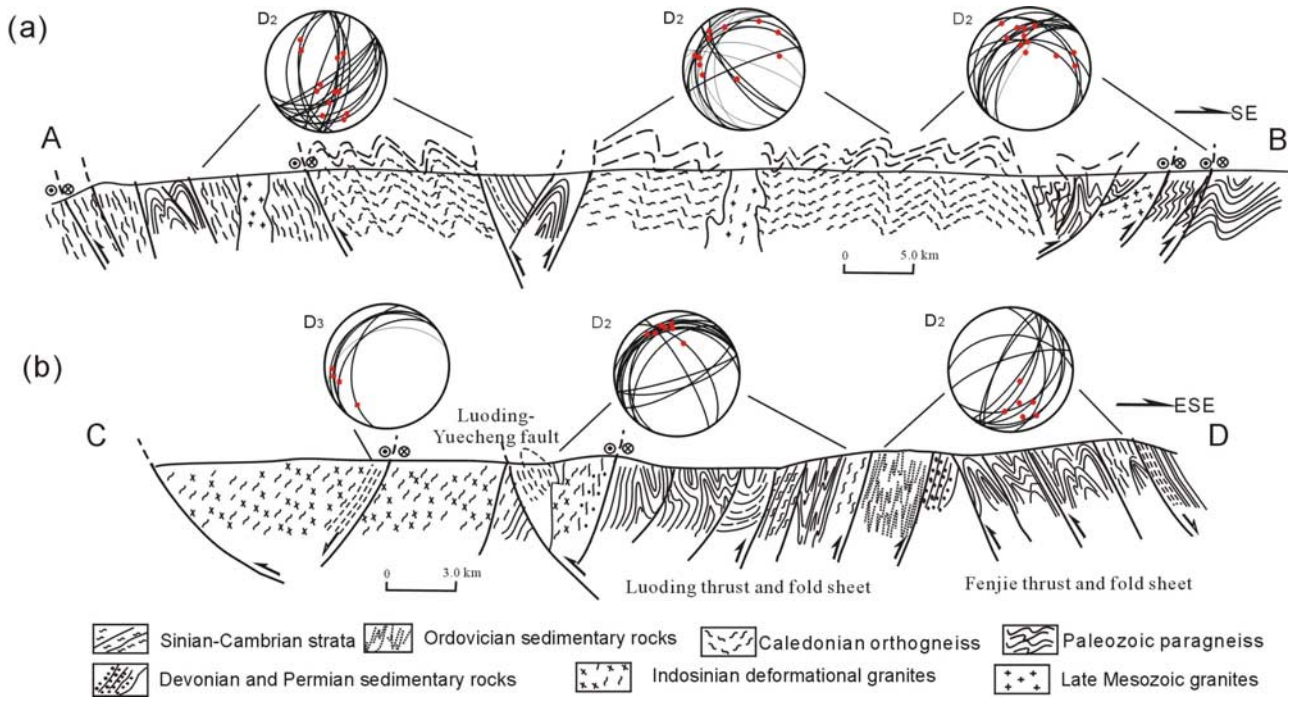

Figure 5. Structural styles along the sections (a) A-B and (b) C-D through the major structural elements of the Yunkaidashan tectonic Belt. See Figure 1b for the locations of theses sections. The stereograms (lower hemisphere, equal area) are also shown for the lineations and foliations of D_2 and D_3.

metamorphic rocks and amphibolites, and by foliation-parallel oriented leucosomes and preferred orientation of biotite in migmatite. D_1 also includes rootless and hook-like folds and structural relicts in the lower Paleozoic sequences that have been largely transposed by later deformation events. D_1 structures are absent from the 467–413 Ma Caledonian granites. The latest deformation (D_4) is characterized by the development of dip-slip faults and drag folds. It affects Jurassic strata and early Yanshanian granites and thus is ascribed to the late Yanshanian event or later. Deformation events D_2 and D_3, which are focus of the current study, are ascribed to the Indosinian orogeny and are mainly developed in the Caledonian plutons and upper Paleozoic strata.

4.1. Deformational Phase D_2

[14] D_2 structural elements are dominated by folds at various scales, fold-and-thrust sheets, an S_2 foliation and L_2 lineation. The fabrics are common throughout the Yunkaidashan Belt, in particular, in the Xinyi-Gaozhou tectonic unit.

[15] D_2 folds have wavelengths ranging from tens of centimeters to a few meters, even up to kilometers. They are overturned, recumbent, and tight (Figures 4a and 4b) and are commonly accompanied by faulting along their limbs. Most folds exhibit asymmetrical Z-shape geometries with axial planes range from SE-SSE dipping in the west to the NW-NNW dipping in the east with the change in orientation occurring approximately along the line of the Xinyi-Liangjiang fault (Figure 5a; see also sections A-B in Figures 2 and 3). The D_2-related faults strike predominantly NE (~30°–60°) and have moderate to steep dips. They result in displacement of high-grade metamorphic rocks (e.g., migmatites, paragneisses and orthogneisses) over low-grade metamorphic Devonian and Carboniferous sandstones and schists, as shown in the Luoding and Fenjie thrust and fold sheets (Figure 5b) [*Peng et al.*, 1996], consistent with a thrusting component in the D_2 domains. The amount of displacement along these faults is not however constrained.

[16] At the northern segment of the Xinyi-Gaozhou tectonic unit, thrust-related folding is well developed [e.g., *Peng et al.*, 1996; *Zhang and Yu*, 1994]. It mainly includes the Luoding and Fenjie thrust and fold sheets in which faults and associated axial planes of folds dip moderately to steeply toward NW and SE respectively, and a series of individual horses stacked on top of each other [e.g., *Peng et al.*, 1996], within each thrust sheet (Figure 5b). Moderately SE-ESE-dipping thrust faults are dominant northwest of the Luoding thrust sheet (see Figures 1c and 5) whereas moderately to steeply NW-dipping thrust faults are characteristic of the region southeast of the Feijie thrust sheet (Figures 1c, and see also section A-B in Figure 2). The coplanar orientation of the D_2 folds and related faults suggest they were contemporaneous, and define a flower-like structural pattern.

[17] S_2 foliations are developed throughout the metamorphic rocks. A moderately to steeply dipping foliation (35°–65°) is defined by compositional layering and preferred orientation of platy minerals in metasedimentary rocks and

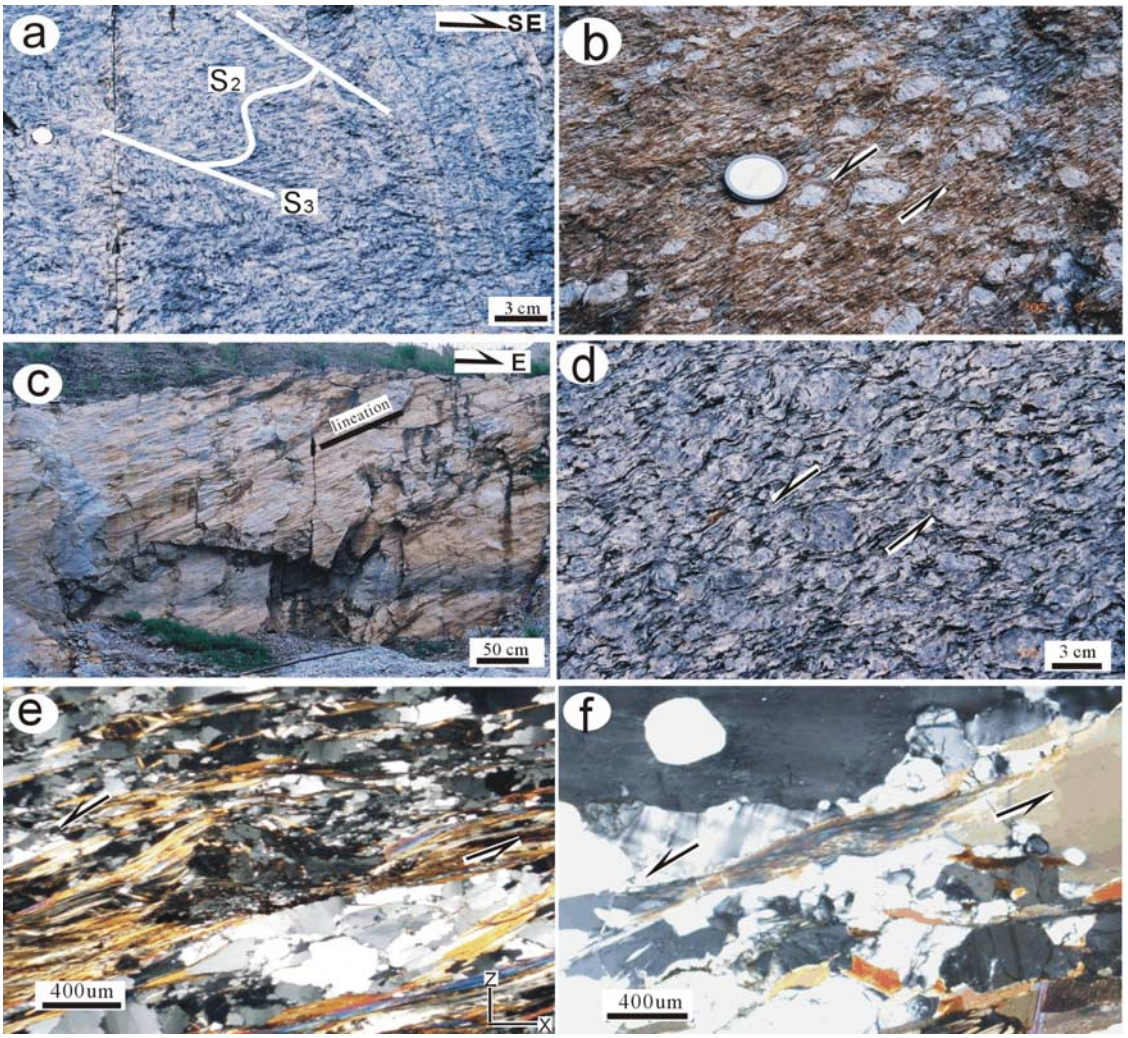

Figure 6. Photos showing D_3 structural elements in the Yunkaidashan tectonic Belt. (a) An overprinting relationship showing S_3 cutting S_2 (Shuanggou, Yangchun). (b) A shallowly plunging L_3 lineation toward the SW (Fengshan, Bobai). Indicatives of sinistral shear sense from (c, d) outcrop and (e, f) microscope, respectively (Figure 6c: north of Baishi, Xinyi; Figure 6d: Linwei, Bobai; Figure 6e: east of Yongning, Yangchun; and Figure 6f: Licun, Rongxian).

by quartz and feldspar ribbons in the orthogneisses. On the basis of our field mapping and data from 1:200 000-scale geological maps, the strike of S_2 foliations are shown in Figure 1c and suggest an original overall NE strike with regions of anomalous orientations related to D_3 deformation. L_2 is an aggregate or grain lineation, which generally plunges at moderate angles (20°–45°, Figures 2, 3, and 5) to the NW-WNW in the eastern part of the Yunkaidashan belt and to the SE-ESE in the western part of belt.

[18] Quartzofeldspathic mylonites developed in the D_2 domains occur in the thrust zone and the overlying nappe. Kinematic indicators in the mylonites, for example, quartzofeldspathic aggregates, en echelon quartz veins and S-shaped asymmetric folds, S-C fabrics, mica fish, elongate quartz, asymmetric porphyroblasts with recrystallized tails and antithetical microfaulted feldspar (Figures 4c–4f), are abundant and generally indicate a sinistral sense of shear. The recrystallized feldspar and hornblende porphyroblasts occur locally in the amphibolite-facies rocks. Quartz c-axis orientation of five mylonitic samples (02YK-90, −50, −59, −69 and −104) associated with D_2 deformation were measured using a universal stage and exhibit monoclinic point-maximum asymmetry with respect to the foliation and lineation (Figures 2 and 3). They have additional maxima close to the *Y* axis along the oblique girdle besides densely populated maxima near the *Z* axis. Such patterns indicate D_2 slipping on the rhombhedral planes $\{r\}\langle a\rangle$ and $\{z\}\langle a\rangle$ under a thermal path ranging from ~550°C to ~300°C, on the basis of polycrystal-plasticity models and experimental studies [*Tullis et al.*, 1973; *Twiss and Moores*, 1994]. The transfor-

mation of biotite and feldspar to phyllosilicates, particularly to chlorite, sericite and muscovite is locally observed, and the phyllosilicates are aligned along the S_2 foliation, suggesting that D_2 deformation likely continued to relatively low temperatures [*Yardley*, 1989]. These data indicate a roughly NW-SE directional shortening with a subsidiary strike-slip component (sinistral) for D_2 deformation under the amphibolite- to greenschist-facies conditions.

4.2. Deformational Phase D_3

[19] All domains with well-preserved D_2 structures were heterogeneously affected by D_3 deformation, especially in the Wuchuang-Sihui and Fengshan-Qinxi shear zones (Tenglong, Luoyangyu, Shanping, Yongning, Shanjia, Kuigang, Shuanggao, Songwan, Wendi, Linwei, Linshan and Licun areas; see Figures 1c, 2, and 3). Field observations show that the most prominent D_3 fabrics include an S_3 mylonitic foliation, L_3 stretching lineation, some reactived-D_2 folds, and low-angle normal faults.

[20] D_3 folds include open to close folds with steep axial planes and folded S_2 foliations. In comparison with D_2 folds, these folds generally occur at smaller meter scales. Kink bands with axes plunging shallowly are locally observed in metasedimentary rocks. Sheath folds and small-scale overturned folds with an axial plane subparallel to the S_3 foliation occur in the Wuchuang-Sihui and Fengshan-Qinxi shear zones, but locally also in the Xinyi-Gaozhou tectonic unit. The fold axes, which are parallel to the newly developed L_3 lineation, plunge subhorizontally or shallowly toward the SSE or the NNW.

[21] S_3 foliation is pervasive and consists of muscovite, biotite, and elongated quartz grains, with L_3 stretching lineation defined by elongated and preferentially oriented quartz and feldspar grains. S_3 is observed to overprint S_2 (Figure 6a) and compared to S_2, it generally has a gentler dip and is associated with lower grade metamorphic assemblages, although both have similar strikes (Figures 1c, 2, and 3). In contrast to L_2, associated L_3 lineation is subhorizontally to shallowly plunging. The geometries of S_3 foliation and L_3 lineation exhibit clear differences between the Wuchuang-Sihui and Fengshan-Qinxi shear zones. In the Wuchuang-Sihui shear zone, S_3 foliation dips moderately toward the SE-ESE, with L_3 lineation subhorizontally to shallowly plunging toward the NE-NNE (Figure 2). A northeasterly trending gneissic banding is parallel to numerous pegmatite veins in the Shaniutang-Yongning area, some of which are strongly boudinaged under high greenschist-facies metamorphism (Figure 2). S_3 foliation in the Fengshan-Qinxi shear zone is generally NE-trending and dips shallowly to moderately toward the NW-WNW, with L_3 plunging subhorizontally to shallowly ($0°-15°$) toward the SW-SSW (Figures 3 and 6b). Fold axis orientations show similar variations. In the Xinyi-Gaozhou tectonic unit, the fabric includes ENE-trending S_3 foliation and refolded S_2 foliation that were probably formed by the sinistral shear sense along the Wuchuang-Sihui and Fengshan-Qinxi shear zones (Figure 1c). All indicators give a sinistral shearing sense in an extensional regime during the D_3 event.

[22] Kinematic indicators associated with D_3 (e.g., mica fish, S-C fabrics, asymmetric boudins and σ- and δ-objects) suggest a sinistral shear sense (Figures 6c–6f). Similarly quartz c-axis measurements of D_3 mylonitic samples for the Wuchuang-Sihui shear zone (02YK-06, −09, −12, −14, −15, and −94), and for the Fengshan-Qinxi shear zone (02YK-56 and −64; Figures 2 and 3) have patterns suggestive of a sinistral shear sense, and show densely populated maxima relatively near the *Z* axis. Such a pattern is probably indicative of the dominant activation of basal ⟨a⟩ gliding system [*Law*, 1990; *Tullis et al.*, 1973], at temperatures of ∼350°–450°C [*Twiss and Moores*, 1994; *Tullis et al.*, 1973]. This is consistent with that estimated from greenschist-facies metamorphism. The brittle behavior of feldspars (e.g., microfractures and kinked twin planes) and ductile deformation of quartz (e.g., recrystallized and flattened quartz ribbons) also document development of S_3 and L_3 fabrics under low-temperature (greenschist-facies) conditions.

[23] All the structural and microstructural observations suggest that D_3 was contemporaneous with greenschist-facies metamorphism, and developed within a dominantly sinistral strike-slip regime with subsidiary extensional deformation. This deformation pattern is consistent with a transtensional regime.

5. Thermochronological Analyses

[24] Biotites crystallized during the D_2 and D_3 deformations were collected from mylonitic samples for $^{40}Ar/^{39}Ar$ dating to constrain the tectonothermal history of the Yunkaidashan Belt. Care was taken to select samples in which biotites could be easily recovered from each fabric element, for example samples for D_2 biotite were collected from outcrops which lacked obvious D_3 biotite and D_3 samples were only collected from regions with clearly new grown biotite related to this event and easily differentiated from D_2 biotite.

5.1. Analytical Methods

[25] Biotite separates from thirteen mylonitic rocks were dated by $^{40}Ar/^{39}Ar$ incremental heating method. The biotite separates were carefully handpicked and checked under a binocular microscope. Weighted aliquots of samples (∼20 mg) were individually wrapped in aluminum foil packet and stacked in sealed Gd-foil with ZBH-1 biotite (132 Ma [*Sang et al.*, 1996]), and irradiated at the central thimble position of the nuclear reactor (1000 kw) at the Chinese Academy of Atomic Energy Science for 2627 min. A gas-sourced mass spectrometer RGA-10 was used for the argon isotope corrections at the Institute of Geology and Geophysics, the Chinese Academy of Sciences (CAS). The concentrations of ^{36}Ar, ^{37}Ar, ^{38}Ar, ^{39}Ar and ^{40}Ar were corrected for the system blank, for radioactive decay of nucleogenic isotopes, and for minor interference reactions involving Ca, K and Cl following procedures reported by *Lo et al.* [1994]. Detailed analytical procedures followed those described by *Hodges et al.* [1994] and *Sang et al.* [1996].

Table 1. The $^{40}Ar/^{39}Ar$ Incremental Heating Analyses on Biotites for Mylonites Associated With the D_2 Transpressive Shearing From the Yunkaidashan Belt[a]

Temp., °C	$(^{40}Ar/^{39}Ar)_m$	$(^{36}Ar/^{39}Ar)_m$	$(^{37}Ar/^{39}Ar)_m$	$(^{38}Ar/^{39}Ar)_m$	$^{39}Ar_k$ (10^{-12}mol)	$(^{40}Ar/^{39}Ar_k)$ ($\pm1\sigma$)	$^{39}Ar_k$ %	Apparent Age (t $\pm1\sigma$Ma)
				02YK[b]				
410	25.247	0.0388	0.2929	0.1035	4.592	13.83 ± 0.039	1.83	289.39 ± 11.02
530	10.188	0.0131	0.1153	0.0437	14.15	6.340 ± 0.007	5.65	138.37 ± 1.86
640	13.144	0.0157	0.1785	0.0681	11.06	8.534 ± 0.012	4.42	183.93 ± 2.96
750	12.985	0.0074	0.1418	0.0544	15.54	10.80 ± 0.011	6.21	229.77 ± 3.53
840	12.769	0.0064	0.1360	0.0484	18.09	10.89 ± 0.011	7.23	231.62 ± 3.47
920	11.604	0.0030	0.0693	0.0294	37.58	10.70 ± 0.008	15.0	227.75 ± 3.12
1000	11.596	0.0027	0.1125	0.0361	41.98	10.79 ± 0.008	16.7	229.57 ± 3.17
1080	11.946	0.0033	0.1184	0.0399	34.56	10.96 ± 0.009	13.8	233.08 ± 3.29
1160	11.904	0.0039	0.1293	0.0408	29.22	10.48 ± 0.009	11.6	228.68 ± 3.23
1240	12.500	0.0056	0.1697	0.0481	20.41	10.84 ± 0.010	8.15	230.58 ± 3.40
1320	13.220	0.0084	0.1987	0.0584	13.68	10.74 ± 0.011	5.47	228.63 ± 3.59
1420	14.425	0.0125	0.2622	0.0737	9.278	10.77 ± 0.014	3.70	229.18 ± 3.99
				02YK-30[c]				
410	19.247	0.0212	0.2634	0.0703	6.564	13.03 ± 0.023	2.22	276.44 ± 6.67
530	10.367	0.0148	0.1158	0.0378	15.63	6.012 ± 0.007	5.29	132.78 ± 1.78
650	12.505	0.0066	0.0977	0.0387	20.18	10.48 ± 0.009	6.83	225.58 ± 3.29
750	11.822	0.0049	0.0946	0.0381	28.25	10.38 ± 0.008	9.56	223.48 ± 3.14
830	11.491	00033	0.0701	0.0256	41.98	10.52 ± 0.008	14.2	226.31 ± 3.08
920	11.343	0.0029	0.0770	0.0286	46.62	10.47 ± 0.007	15.7	225.28 ± 3.05
1000	11.616	0.0037	0.0919	0.0332	37.30	10.52 ± 0.008	12.6	226.41 ± 3.12
1080	11.765	0.0042	0.0946	0.0349	32.84	10.52 ± 0.008	11.1	226.42 ± 3.15
1160	12.095	0.0057	0.1143	0.0348	24.35	10.42 ± 0.009	8.24	224.33 ± 3.18
1240	12.791	0.0081	0.1141	0.0440	17.11	10.41 ± 0.010	5.79	224.10 ± 3.35
1320	14.414	0.0135	0.2230	0.0529	10.29	10.45 ± 0.013	3.48	225.05 ± 3.78
1430	13.431	0.0098	0.1561	0.0482	14.19	10.56 ± 0.011	4.80	227.12 ± 3.55
				02YK-74[d]				
400	19.679	0.0246	0.3137	0.0901	4.708	12.46 ± 0.024	2.01	262.67 ± 6.70
500	10.440	0.0142	0.1062	0.0366	15.51	6.271 ± 0.007	6.62	136.93 ± 1.84
600	14.950	0.0214	0.1850	0.0735	10.85	8.683 ± 0.014	4.63	186.94 ± 3.40
700	12.900	0.0076	0.1458	0.0603	15.19	10.66 ± 0.011	6.48	227.10 ± 3.51
780	12.631	0.0065	0.1432	0.0572	17.63	10.71 ± 0.010	7.52	227.91 ± 3.45
860	11.520	0.0029	0.1123	0.0348	39.66	10.66 ± 0.008	16.9	227.10 ± 3.12
940	11.580	0.0032	0.1117	0.0345	35.95	10.64 ± 0.008	15.3	216.52 ± 3.12
1020	11.967	0.0040	0.1210	0.0405	28.30	10.77 ± 0.009	12.0	229.15 ± 3.25
1100	12.261	0.0050	0.1250	0.0477	23.08	10.79 ± 0.009	9.85	229.60 ± 3.34
1200	12.500	0.0059	0.1256	0.0447	19.48	10.76 ± 0.010	8.32	228.91 ± 3.36
1300	13.098	0.0081	0.1529	0.0500	14.15	10.70 ± 0.011	6.04	227.73 ± 3.50
1400	14.168	0.0120	0.1953	0.0638	9.626	10.64 ± 0.013	4.11	226.57 ± 3.81
				02YK-38[e]				
460	22.325	0.0307	0.2245	0.0850	5.13	13.29 ± 0.031	1.69	278.77 ± 8.56
560	8.310	0.0071	0.0680	0.0280	19.48	6.212 ± 0.004	6.44	135.61 ± 1.68
640	12.769	0.0076	0.0857	0.0329	18.09	10.51 ± 0.010	5.98	223.84 ± 3.30
720	12.180	0.0062	0.0825	0.0348	22.13	10.33 ± 0.009	7.32	220.31 ± 3.14
800	11.506	0.0041	0.0639	0.0267	33.26	10.27 ± 0.008	11.0	221.17 ± 2.99
880	11.455	0.0037	0.0650	0.0257	37.30	10.36 ± 0.008	12.3	220.81 ± 3.00
960	11.465	0.0033	0.0874	0.0322	41.47	10.48 ± 0.008	13.7	223.28 ± 3.05
1040	11.561	0.0039	0.0888	0.0319	35.21	10.40 ± 0.008	11.6	221.69 ± 3.05
1120	11.742	0.0042	0.0909	0.0317	32.47	10.48 ± 0.008	10.7	221.37 ± 3.10
1200	11.882	0.0051	0.1043	0.0325	26.86	10.36 ± 0.008	8.88	220.91 ± 3.09
1300	12.560	0.0072	0.1212	0.0413	19.20	10.43 ± 0.009	6.35	222.37 ± 3.27
1400	13.975	0.0120	0.1646	0.0534	11.55	10.44 ± 0.012	3.82	222.52 ± 3.63
				02YK-39[f]				
410	24.395	0.0373	0.2508	0.0580	6.216	13.44 ± 0.036	2.32	284.45 ± 10.1
530	13.106	0.0202	0.1697	0.0521	10.85	7.150 ± 0.011	4.06	156.84 ± 2.46
650	12.575	0.0075	0.1352	0.0414	15.31	10.35 ± 0.010	5.72	223.02 ± 3.28
750	12.209	0.0058	0.1123	0.0366	19.95	10.50 ± 0.009	7.46	226.04 ± 3.23
840	11.826	0.0043	0.0935	0.0317	26.67	10.55 ± 0.008	9.98	226.97 ± 3.16
920	11.419	0.0032	0.0890	0.0278	35.95	10.47 ± 0.008	13.4	225.41 ± 3.06
1000	11.161	0.0025	0.0839	0.0280	45.93	10.42 ± 0.007	17.1	224.36 ± 3.01
1080	11.266	0.0030	0.0979	0.0314	37.92	10.37 ± 0.007	14.1	223.33 ± 3.02

Table 1. (continued)

Temp., °C	$(^{40}Ar/^{39}Ar)_m$	$(^{36}Ar/^{39}Ar)_m$	$(^{37}Ar/^{39}Ar)_m$	$(^{38}Ar/^{39}Ar)_m$	$^{39}Ar_k$ (10^{-12}mol)	$(^{40}Ar/^{39}Ar_k)$ ($\pm1\sigma$)	$^{39}Ar_k$ %	Apparent Age (t $\pm1\sigma$Ma)
1160	11.481	0.0037	0.1032	0.0328	31.31	10.39 ± 0.008	11.7	223.86 ± 3.07
1240	12.337	0.0064	0.1619	0.0489	17.86	10.44 ± 0.009	6.68	224.71 ± 3.30
1320	13.148	0.0092	0.1878	0.0585	12.52	10.44 ± 0.011	4.68	224.71 ± 3.51
1420	19.993	0.0243	0.2885	0.0961	6.680	10.87 ± 0.025	2.49	273.24 ± 7.16

[a]Parameter $\lambda = 5.543e^{-10}$/a, $(^{40}Ar/^{39}Ar)_m$: measured values of $^{40}Ar/^{39}Ar$, $^{39}Ar_k$: measured values of $^{39}Ar_k$, which was produced by k decay.
[b]J is 0.012573, weight is 0.0979 g, and plateau age (steps 4–12) is 229.9 ± 0.5 Ma. Inverse isochron age is 229.8 ± 0.4 Ma, $^{40}Ar/^{36}Ar$ ratio is 292.35, and MSWD is 1.82.
[c]J is 0.012703, weight is 0.1022 g, and plateau age (steps 3–11) is 225.4 ± 0.3 Ma. Inverse isochron age is 225.5 ± 0.4 Ma, $^{40}Ar/^{36}Ar$ ratio is 292.2, and MSWD is 1.76.
[d]J is 0.012573, weight is 0.1017 g, and plateau age (steps 4–12) is 227.9 ± 0.3 Ma. Inverse isochron age is 228.4 ± 0.4 Ma, $^{40}Ar/^{36}Ar$ ratio is 290.6, and MSWD is 1.24.
[e]J is 0.012566, weight is 0.1045 g, and plateau age (steps 4–12) is 221.8 ± 0.4 Ma. Inverse isochron age is 220.6 ± 0.4 Ma, $^{40}Ar/^{36}Ar$ ratio is 303.5, and MSWD is 4.06.
[f]J is 0.012703, weight is 0.0929 g, and plateau age (steps 4–11) is 224.7 ± 0.4 Ma. Inverse isochron age is 224.5 ± 0.4 Ma, $^{40}Ar/^{36}Ar$ ratio is 294.6, and MSWD is 1.27.

5.2. Biotite $^{40}Ar/^{39}Ar$ Dating Results

[26] The $^{40}Ar/^{39}Ar$ dating results are listed in Tables 1 and 2 and are plotted as age spectra in Figures 7 and 8. A summary of the sampling locations, lithology and corresponding geochronological results is given in Figures 1c, 2 and 3, and Table 3. Plateau ages are based on three requirements: (1) at least six successive temperature steps fall within 1σ of the average; (2) the gas fractions for these plateau steps must comprise more than 70% of total ^{39}Ar released; and (3) the plateau age should be concordant with its $^{40}Ar/^{39}Ar$ dates and $^{40}Ar/^{36}Ar$ intercept values be reasonable.

5.2.1. D_2-Related Mylonites

[27] D_2-related mylonitic samples of Caledonian granitic gneisses (02YK-27, −30 and −38) were taken from Hebapu (Xinyi), Baishi (Xinyi) and Dongping (Gaozhou), respectively. In thin section, elongated quartz ribbons and oriented muscovite and biotite flakes are present. The microstructures, together with variations of mylonitic foliation and lineation indicate a thrusting with sinistral strike-slip component under greenschist- to low amphibolite-facies conditions. Biotites aligned along the foliation crystallized under greenschist-facies metamorphism during the D_2 event. Biotite separates for 02YK-27, −30 and −38 yield flat $^{40}Ar/^{39}Ar$ apparent age spectra, giving the plateau ages of 229.9 ± 0.5 Ma, 225.4 ± 0.3 Ma and 221.8 ± 0.4 Ma defined by >85% released gas, respectively (Figures 7a–7c). Regressions of plateau step data also suggest $^{40}Ar/^{36}Ar$ initial values of 292.2–303.5, which are close to the present-day atmospheric values (295.5). The intercept dates of 229.8 ± 0.4 Ma, 225.5 ± 0.4 Ma and 220.6 ± 0.4 Ma are concordant with their respective plateau ages with statistically meaningful MSWD values (Tables 1, 2, and 3).

[28] Mylonitic migmatite 02YK-39 was collected from Xieji village (Gaozhou) and mylonitic paragneiss 02YK-74 was from 2 km north of Xinyi city. Both samples exhibit D_2 transpressional fabrics. Biotite separates yield the well-defined plateau ages of 227.9 ± 0.3 Ma and 224.7 ± 0.4 Ma for intermediate-high temperature heating steps, respectively (Figures 7d and 7e).

5.2.2. D_3-Related Mylonites

[29] Three mylonitic samples associated with D_3 deformation were taken from Puzhou (Yangchun, 02YK-9), Shaniutang (Yangchun, 02YK-12) and 3 km west of Yongning (Yangchun, 02YK-15) in the Wuchuang-Sihui shear zone. D_3 mylonite samples 02YK-56, −64 and −80 were collected from Lingwei (Bobai), Licun (Rongxian) and Tengbin (Luoding), respectively within the Fengshan-Qinxi shear zone. They exhibit NE/ENE-trending moderately or steeply mylonitic foliations with subhorizontally to shallowly plunging stretching lineations, and contain quartz ribbons, feldspar sigma, delta clasts and mica fish that indicate a sinistral shear sense. Biotites occur within shear planes and as small grains delineating the stretching lineation. All the biotite separates from the samples yield well-defined plateau ages during intermediate to high temperature heating steps (Figures 8a–8f) with ages of 207.8 ± 0.2 Ma (02YK-9), 209.0 ± 0.2 Ma (02YK-12), 211.5 ± 0.5 Ma (02YK-15), 218.4 ± 0.3 Ma (02YK-56), 211.1 ± 0.2 Ma (02YK-64) and 208.9 ± 1.4 Ma (02YK-80), respectively. The biotite separates for two D_3-related mylonitic samples from Qianpai (Xinyi, 02YK-26) and 7 km north of Baishi (Xinyi, 02YK-31) in the Xinyi-Gaozhou tectonic unit, were also analyzed and yield well-defined plateau ages of 214.2 ± 0.4 Ma and 216.9 ± 0.3 Ma, respectively (Figures 8g and 8h). These ages are defined by more than 83% of total ^{39}Ar release, and have $^{40}Ar/^{36}Ar$ initial ratios of 283–309. The corresponding inverse isochron ages are consistent with their plateau ages (Tables 1, 2, and 3).

6. Discussion and Conclusions

6.1. Timing Constrains of D_2 and D_3 Deformation

[30] The closure temperature for argon retention in biotite is generally believed to be in range of ~300°–350°C across a range of cooling rates and chemical compositions [*Purdy and Jäger*, 1976; *Dodson*, 1973; *Harrison et al.*, 1985]. The

Table 2. The $^{40}Ar/^{39}Ar$ Incremental Heating Analyses on Biotites for Mylonites Associated With the D_3 Transpressive Shearing From the Yunkaidashan Belt[a]

Temp., °C	$(^{40}Ar/^{39}Ar)_m$	$(^{36}Ar/^{39}Ar)_m$	$(^{37}Ar/^{39}Ar)_m$	$(^{38}Ar/^{39}Ar)_m$	$^{39}Ar_k$ (10^{-12}mol)	$(^{40}Ar/^{39}Ar_k)$ ($\pm1\sigma$)	$^{39}Ar_k$ %	Apparent Age ($t \pm1\sigma$Ma)
				02YK-9[b]				
400	25.020	0.0408	0.2412	0.0714	1.683	13.03 ± 0.038	1.91	275.15 ± 10.2
500	9.864	0.0128	0.0939	0.0336	16.19	6.077 ± 0.006	5.46	133.50 ± 1.75
600	16.710	0.0287	0.1696	0.0665	9.696	8.281 ± 0.017	3.27	179.58 ± 3.66
700	12.500	0.0095	0.0920	0.0396	19.48	9.705 ± 0.009	6.58	208.74 ± 3.06
800	11.386	0.0058	0.0682	0.0346	31.78	9.674 ± 0.008	10.7	208.09 ± 2.85
880	10.939	0.0044	0.0563	0.0296	41.99	9.642 ± 0.007	14.1	207.45 ± 2.77
960	10.409	0.0027	0.0756	0.0407	51.03	9.613 ± 0.007	17.2	206.86 ± 2.74
1040	10.731	0.0036	0.0923	0.0435	38.04	9.663 ± 0.007	12.8	207.88 ± 2.80
1120	11.154	0.0049	0.0991	0.0489	32.94	9.713 ± 0.008	11.1	208.90 ± 2.90
1200	12.040	0.0082	0.1261	0.0584	22.73	9.651 ± 0.010	7.67	207.64 ± 3.07
1300	13.095	0.0119	0.1311	0.0644	15.58	9.606 ± 0.012	5.26	206.72 ± 3.28
1400	14.638	0.0170	0.1669	0.0665	10.90	9.647 ± 0.014	3.68	207.55 ± 3.63
				02YK-12[c]				
460	13.065	0.0295	0.2158	0.0908	7.07	4.406 ± 0.013	2.50	97.78 ± 1.70
560	9.073	0.0105	0.1062	0.0427	17.51	5.964 ± 0.005	6.18	131.11 ± 1.70
640	13.868	0.0182	0.1632	0.0698	12.71	8.516 ± 0.013	4.49	184.43 ± 3.11
720	12.800	0.0106	0.1330	0.0553	17.39	9.674 ± 0.011	6.14	208.10 ± 3.18
800	11.904	0.0076	0.1155	0.0440	24.35	9.673 ± 0.009	8.60	208.08 ± 2.97
880	10.645	0.0032	0.0740	0.0341	43.14	9.701 ± 0.007	15.2	208.66 ± 2.76
950	10.555	0.0027	0.0728	0.0364	50.10	9.744 ± 0.007	17.7	209.52 ± 2.77
1020	11.006	0.0044	0.0860	0.0369	36.88	9.718 ± 0.007	13.0	208.99 ± 2.82
1100	11.287	0.0053	0.0942	0.0335	30.62	9.735 ± 0.008	10.8	209.33 ± 2.85
1200	12.117	0.0082	0.1125	0.0430	19.71	9.704 ± 0.009	6.96	208.71 ± 3.01
1300	12.539	0.0095	0.1338	0.0468	14.61	9.749 ± 0.010	5.16	209.63 ± 3.11
1400	14.421	0.0157	0.1975	0.0560	8.81	9.794 ± 0.013	3.11	210.53 ± 3.57
				02YK-15[d]				
450	16.951	0.0278	0.2739	0.0818	6.657	8.777 ± 0.018	2.24	189.88 ± 4.01
550	8.891	0.0101	0.1147	0.0368	18.23	5.905 ± 0.005	6.15	129.91 ± 1.65
650	12.151	0.0075	0.1234	0.0417	18.32	9.928 ± 0.009	6.18	213.34 ± 3.07
730	11.395	0.0054	0.0893	0.0295	29.92	9.805 ± 0.008	10.1	210.85 ± 2.87
800	11.118	0.0046	0.0827	0.0289	35.26	9.769 ± 0.007	11.9	210.12 ± 2.82
870	10.804	0.0030	0.0922	0.0298	46.16	9.923 ± 0.007	15.5	213.25 ± 2.82
940	10.790	0.0034	0.1158	0.0366	39.90	9.773 ± 0.007	13.4	210.21 ± 2.81
1020	10.960	0.0039	0.1103	0.0355	35.26	9.808 ± 0.007	11.9	210.91 ± 2.84
1100	11.790	0.0070	0.1208	0.0434	26.16	9.714 ± 0.009	8.83	209.01 ± 2.96
1200	12.878	0.0101	0.1654	0.0517	18.37	9.922 ± 0.010	6.20	213.22 ± 3.25
1320	13.372	0.0116	0.1370	0.0421	15.96	9.963 ± 0.011	5.39	214.05 ± 3.32
1440	19.743	0.0276	0.3024	0.0830	5.868	11.63 ± 0.024	1.98	247.58 ± 6.33
				02YK-26[e]				
420	14.298	0.0179	0.17373	0.0492	7.77	9.044 ± 0.012	2.72	194.24 ± 3.25
550	8.8187	0.0101	0.08710	0.0259	18.30	5.841 ± 0.004	6.42	127.81 ± 1.60
630	13.323	0.0185	0.15432	0.0520	12.24	7.877 ± 0.011	4.29	170.31 ± 2.70
700	12.073	0.0073	0.10840	0.0408	19.02	9.929 ± 0.009	6.67	212.17 ± 3.04
780	11.636	0.0054	0.09331	0.0359	25.51	10.03 ± 0.008	8.95	214.37 ± 2.98
860	11.289	0.0041	0.07760	0.0303	33.82	10.08 ± 0.007	11.8	215.28 ± 2.92
940	10.821	0.0028	0.08480	0.0239	48.02	9.974 ± 0.007	16.8	213.06 ± 2.81
1020	11.301	0.0042	0.10900	0.0339	32.43	10.04 ± 0.008	11.3	214.54 ± 2.92
1100	11.488	0.0048	0.11215	0.0351	28.67	10.06 ± 0.008	10.0	214.98 ± 2.96
1180	11.775	0.0056	0.12065	0.0368	24.82	10.13 ± 0.008	8.71	216.32 ± 3.03
1260	12.514	0.0084	0.13900	0.0485	16.42	10.03 ± 0.010	5.76	214.26 ± 3.18
1340	13.333	0.0116	0.16611	0.0556	11.96	9.928 ± 0.011	4.20	212.13 ± 3.35
1440	22.215	0.0313	0.29879	0.0843	5.91	13.01 ± 0.030	2.07	273.34 ± 8.33
				02YK-31[f]				
420	18.406	0.0268	0.1613	0.0724	6.91	10.52 ± 0.021	2.21	224.13 ± 5.16
550	10.743	0.0161	0.0967	0.0394	14.35	5.998 ± 0.007	4.59	131.12 ± 1.79
660	13.308	0.0168	0.1434	0.0620	11.06	8.388 ± 0.011	3.54	180.82 ± 2.91
760	12.287	0.0073	0.1012	0.0437	18.86	10.12 ± 0.009	6.04	216.11 ± 3.14
840	11.204	0.0036	0.0753	0.0261	38.51	10.14 ± 0.007	12.3	216.53 ± 2.91
920	11.005	0.0031	0.0887	0.0345	43.84	10.07 ± 0.007	14.0	215.16 ± 2.89
1000	10.963	0.0027	0.0906	0.0334	50.57	10.16 ± 0.007	16.1	216.81 ± 2.90
1080	11.230	0.0033	0.1002	0.0390	41.29	10.24 ± 0.008	13.2	218.55 ± 2.98

Table 2. (continued)

Temp., °C	$(^{40}Ar/^{39}Ar)_m$	$(^{36}Ar/^{39}Ar)_m$	$(^{37}Ar/^{39}Ar)_m$	$(^{38}Ar/^{39}Ar)_m$	$^{39}Ar_k$ (10^{-12}mol)	$(^{40}Ar/^{39}Ar_k)$ ($\pm1\sigma$)	$^{39}Ar_k$ %	Apparent Age ($t \pm1\sigma$Ma)
1160	11.418	0.0040	0.1018	0.0395	34.33	10.23 ± 0.008	10.9	218.30 ± 3.01
1240	11.785	0.0053	0.1097	0.0477	25.98	10.21 ± 0.009	8.32	218.00 ± 3.10
1340	12.433	0.0079	0.1302	0.0521	17.53	10.11 ± 0.010	5.61	215.82 ± 3.21
1420	14.739	0.0156	0.1948	0.0807	8.91	10.16 ± 0.014	2.85	216.97 ± 3.91
				02YK-56[g]				
420	19.020	0.0234	0.0751	0.0818	6.91	12.12 ± 0.012	2.25	255.75 ± 6.17
540	9.1681	0.0111	0.0291	0.0327	20.83	5.893 ± 0.005	6.80	128.89 ± 1.65
650	13.748	0.0190	0.0619	0.0673	11.55	8.144 ± 0.012	3.77	175.79 ± 2.94
760	12.565	0.0078	0.0456	0.0496	17.63	10.24 ± 0.010	5.75	219.54 ± 3.26
840	11.315	0.0039	0.0258	0.0279	35.26	10.15 ± 0.007	11.5	218.68 ± 2.93
920	11.000	0.0028	0.0315	0.0322	48.71	10.16 ± 0.007	15.9	218.79 ± 2.90
1000	11.216	0.0032	0.0305	0.0333	42.73	10.25 ± 0.007	13.9	218.77 ± 2.96
1080	11.228	0.0035	0.0304	0.0336	39.67	10.19 ± 0.007	12.9	218.53 ± 2.85
1160	11.538	0.0042	0.0340	0.0366	32.57	10.28 ± 0.008	10.6	219.25 ± 3.03
1240	11.895	0.0055	0.0384	0.0433	24.96	10.25 ± 0.009	8.15	219.76 ± 3.11
1340	12.750	0.0085	0.0466	0.0492	16.19	10.22 ± 0.010	5.28	219.11 ± 3.28
1440	14.582	0.0151	0.0706	0.0724	9.16	10.12 ± 0.014	2.99	217.02 ± 3.80
				02YK-64[h]				
450	8.362	0.0086	0.0562	0.0573	10.76	5.832 ± 0.006	3.61	128.36 ± 1.69
550	14.023	0.0232	0.0737	0.0799	9.98	7.191 ± 0.013	3.34	157.01 ± 2.75
650	12.892	0.0104	0.0442	0.0493	17.72	9.816 ± 0.010	5.94	211.08 ± 3.21
720	11.985	0.0074	0.0332	0.0387	24.77	9.793 ± 0.009	8.31	210.42 ± 2.99
800	11.680	0.0063	0.0321	0.0348	28.99	9.799 ± 0.008	9.73	210.73 ± 2.93
870	10.829	0.0034	0.0293	0.0331	40.27	9.814 ± 0.007	13.5	211.04 ± 3.81
940	10.585	0.0027	0.0314	0.0349	51.50	9.792 ± 0.007	17.2	210.59 ± 2.78
1020	11.125	0.0043	0.0363	0.0434	37.11	9.841 ± 0.008	12.4	211.58 ± 2.90
1100	11.428	0.0052	0.0400	0.0424	30.85	9.883 ± 0.008	10.3	211.44 ± 2.95
1200	11.826	0.0067	0.0481	0.0473	24.12	9.851 ± 0.009	8.09	211.79 ± 3.03
1300	12.388	0.0089	0.0581	0.0497	15.54	9.759 ± 0.010	5.21	209.92 ± 3.10
1400	20.959	0.0295	0.1169	0.1044	6.29	12.59 ± 0.028	2.10	260.61 ± 7.41
				04YK-80[i]				
300	16.994	0.0263	0.01375	0.0276	0.096	9.208 ± 0.480	0.87	215.29 ± 11.30
500	13.781	0.0157	0.00854	0.0091	0.313	9.128 ± 0.150	2.84	213.54 ± 3.48
620	12.887	0.0134	0.00407	0.0100	0.855	8.922 ± 0.068	7.76	208.98 ± 1.59
720	12.515	0.0122	0.00402	0.0056	1.173	8.91 ± 0.065	10.64	208.76 ± 1.52
850	11.339	0.0082	0.00348	0.0041	2.000	8.910 ± 0.074	18.14	208.72 ± 1.73
980	11.004	0.0070	0.00424	0.0054	1.823	8.923 ± 0.073	16.54	209.00 ± 1.70
1050	10.437	0.0052	0.00441	0.0043	2.019	8.892 ± 0.068	18.32	208.31 ± 1.60
1100	10.132	0.0043	0.00733	0.0058	1.459	8.857 ± 0.082	13.24	207.55 ± 1.92
1150	10.774	0.0065	0.01465	0.0121	0.821	8.845 ± 0.0130	7.45	207.28 ± 3.08
1200	11.879	0.0100	0.03930	0.0344	0.255	8.922 ± 0.210	2.31	208.99 ± 4.99
1250	11.559	0.0105	0.01735	0.0669	0.111	8.448 ± 0.150	1.01	233.46 ± 4.09
1300	11.889	0.0119	0.00651	0.0711	0.097	8.347 ± 0.270	0.88	230.84 ± 7.46

[a]Parameter $\lambda = 5.543e^{-10}$/a, $(^{40}Ar/^{39}Ar)_m$: measured values of $^{40}Ar/^{39}Ar$, $^{39}Ar_k$: measured values of $^{39}Ar_k$, which was produced by k decay.

[b]J is 0.012638, weight is 0.1024 g, and plateau age (steps 4–12) is 207.8 ± 0.2 Ma. Inverse isochron age is 207.7 ± 0.3 Ma, $^{40}Ar/^{36}Ar$ ratio is 293.3, and MSWD is 0.66.

[c]J is 0.012638, 02YK-12, weight is 0.0993 g, and plateau age (steps 4–11) is 209.0 ± 0.2 Ma. Inverse isochron age is 208.7 ± 0.3 Ma, $^{40}Ar/^{36}Ar$ ratio is 295.6, and MSWD is 0.71.

[d]J is 0.012644, weight is 0.0988 g, and plateau age (steps 4–11) is 211.5 ± 0.5 Ma. Inverse isochron age is 209.5 ± 0.4 Ma, $^{40}Ar/^{36}Ar$ ratio is 309.4, and MSWD is 5.77.

[e]J is 0.012568, weight is 0.1027 g, and plateau age (steps 4–12) is 214.2 ± 0.4 Ma. Inverse isochron age is 215.2 ± 0.4 Ma, $^{40}Ar/^{36}Ar$ ratio is 283.6, and MSWD is 2.03.

[f]J is 0.012568, weight is 0.1037 g, and plateau age (steps 4–12) is 216.9 ± 0.3 Ma. Inverse isochron age is 217.0 ± 0.4 Ma, $^{40}Ar/^{36}Ar$ ratio is 291.9, and MSWD is 0.89.

[g]J is 0.012566, weight is 0.1031 g, and plateau age (steps 4–12) is 218.4 ± 0.3 Ma. Inverse isochron age is 218.2 ± 0.4 Ma, $^{40}Ar/^{36}Ar$ ratio is 290.4, and MSWD is 1.26.

[h]J is 0.012644, weight is 0.0986 g, and plateau age (steps 3–11) is 211.1 ± 0.2 Ma. Inverse isochron age is 211.4 ± 0.4 Ma, $^{40}Ar/^{36}Ar$ ratio is 291.2, and MSWD is 0.61.

[i]J is 0.013766, weight is 0.1031 g, and plateau age (steps 3–10) is 208.9 ± 1.4 Ma. Inverse isochron age is 208.8 ± 1.2 Ma, $^{40}Ar/^{36}Ar$ ratio is 298.4, and MSWD is 2.31.

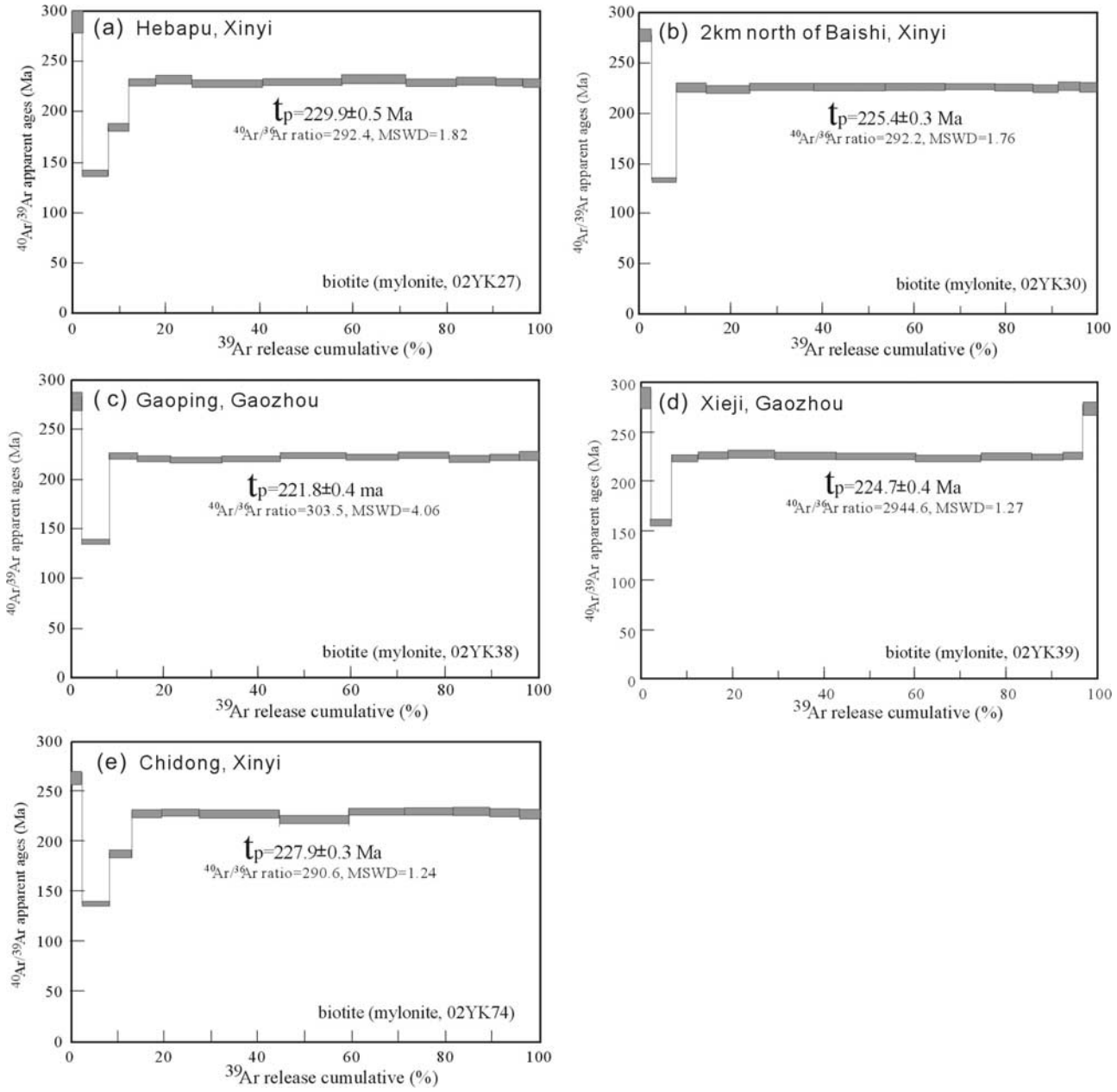

Figure 7. The $^{40}Ar/^{39}Ar$ apparent age spectra of synkinematic biotites from D_2-related mylonitic rocks. (a) 02YK-27 (Hebapu, Xinyi); (b) 02YK-30 (Baishi, Xinyi); (c) 02YK-38 (Dongping, Gaozhou); (d) 02YK-74 (Chidong, Xinyi); and (e) 02YK-39 (Xieji, Gaozhou). Coarse lines give the apparent ages (the length of bars reflects 1σ uncertainty). See Figure 1b for the locations of the samples.

D_2-related deformation structures underwent lower amphibolite- to greenschist-facies metamorphism. This suggests that temperature during the D_2 event was probably close to the argon closure temperature of the synkinematic biotites [e.g., *Hames and Bowring*, 1995; *Harrison et al.*, 1985]. Moreover, a delay between the shearing termination and mica argon closure might be within a short time span (<10 Ma) when assuming a mean cooling rate of at least

Figure 8. The $^{40}Ar/^{39}Ar$ apparent age spectra of synkinematic biotites from mylonitic rocks associated with D_3. Wuchuang-Sihui shear zone: (a) 02YK-9 (Puzhou, Yangchun), (b) 02YK-12 (Shaniutang, Yangchun), and (c) 02YK-15 (3 km west of Yongning, Yangchun). Fengshan-Qinxi shear zone: (d) 02YK-56 (Linwei, Bobai), (e) 02YK-64 (Licun, Rongxian), and (f) 02YK-80 (west of Tengbin, Luoding). Xinyi-Gaozhou tectonic unit: (g) 02YK-26 (Qianpai, Xinyi) and (h) 02YK-31 (7 km north of Baishi, Xinyi). Coarse lines give the apparent ages (the length of bars reflects 1σ uncertainty). See Figures 1b and 3 for the locations of the samples.

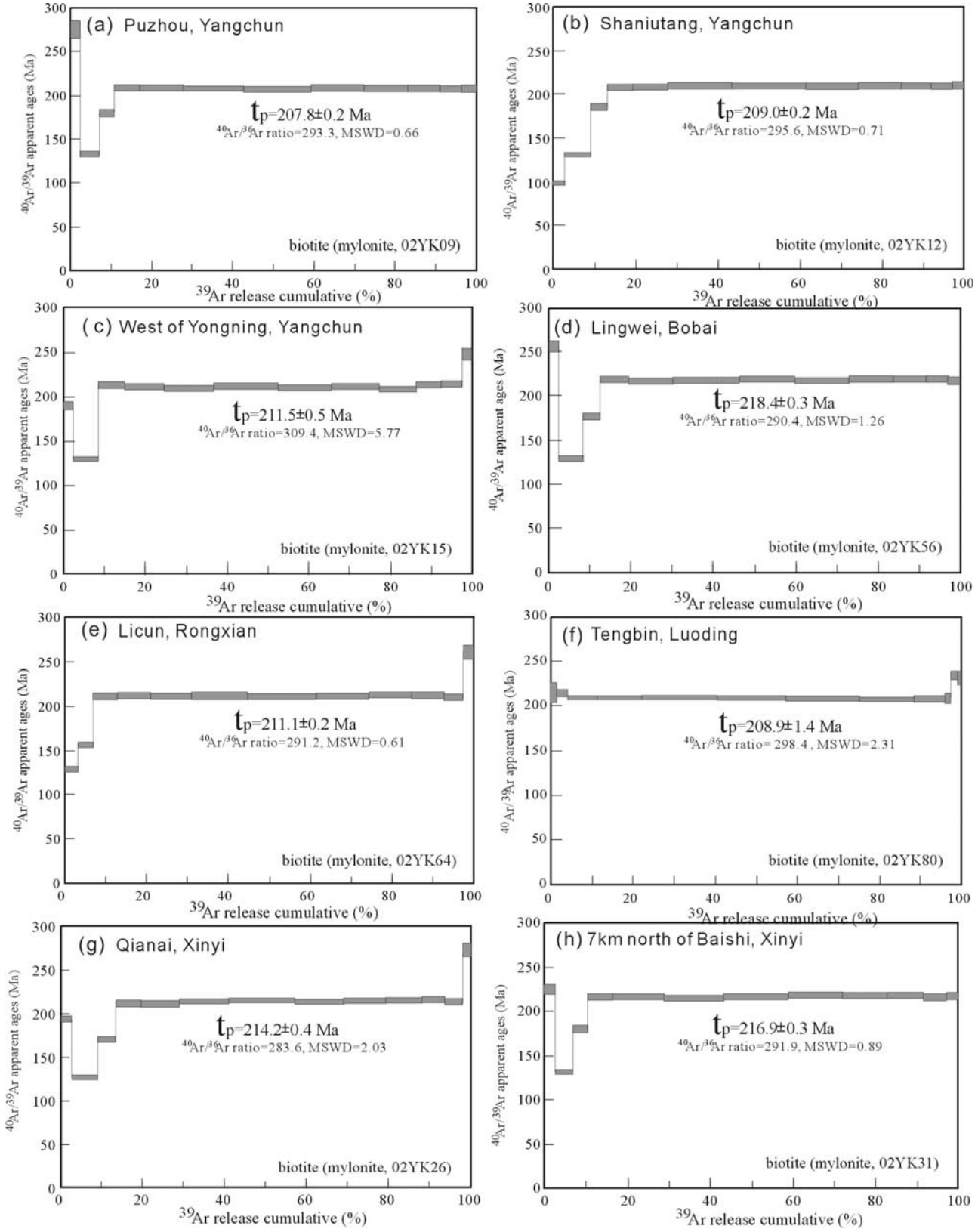
(a) Puzhou, Yangchun
tp=207.8±0.2 Ma
40Ar/36Ar ratio=293.3, MSWD=0.66
biotite (mylonite, 02YK09)
(b) Shaniutang, Yangchun
tp=209.0±0.2 Ma
40Ar/36Ar ratio=295.6, MSWD=0.71
biotite (mylonite, 02YK12)
(c) West of Yongning, Yangchun
tp=211.5±0.5 Ma
40Ar/36Ar ratio=309.4, MSWD=5.77
biotite (mylonite, 02YK15)
(d) Lingwei, Bobai
tp=218.4±0.3 Ma
40Ar/36Ar ratio=290.4, MSWD=1.26
biotite (mylonite, 02YK56)
(e) Licun, Rongxian
tp=211.1±0.2 Ma
40Ar/36Ar ratio=291.2, MSWD=0.61
biotite (mylonite, 02YK64)
(f) Tengbin, Luoding
tp=208.9±1.4 Ma
40Ar/36Ar ratio= 298.4 , MSWD=2.31
biotite (mylonite, 02YK80)
(g) Qianai, Xinyi
tp=214.2±0.4 Ma
40Ar/36Ar ratio=283.6, MSWD=2.03
biotite (mylonite, 02YK26)
(h) 7km north of Baishi, Xinyi
tp=216.9±0.3 Ma
40Ar/36Ar ratio=291.9, MSWD=0.89
biotite (mylonite, 02YK31)
40Ar/39Ar apparent ages (Ma)
39Ar release cumulative (%)

Figure 8

Table 3. Summary of Locations and $^{40}Ar/^{39}Ar$ Geochronology for the Yunkaidashan Belt

Sample	Location	Rock Type	Longitude, Latitude	Biotite $^{40}Ar/^{39}Ar$ Age (Ma ± 1σ)				
				Plateau Age (Steps)	Intercept Data	$^{39}Ar_k$, %	$(^{40}Ar/^{36}Ar)_i$	MSWD
			D_2-Related Mylonites					
02YK-27	Hebapu, Xinyi	mylonitic granite	111°09′15″ 22°22′38″	229.9 ± 0.5 (4–12)	229.8 ± 0.4	87.7	292.4	1.82
02YK-30	5 km north of Baishi	granitic mylonite	111°04′39″ 22°24′32″	225.4 ± 0.3 (3–12)	225.5 ± 0.4	87.5	292.2	1.76
02YK-38	Dongping, Gaozhou	mylonitic gneiss	110°55′11″ 21°54′30″	221.8 ± 0.4 (4–12)	220.6 ± 0.4	85.7	303.5	4.06
02YK-74	2 km north of Xinyi	mylonitic paragneiss		227.9 ± 0.3 (4–12)	228.4 ± 0.4	86.5	290.6	1.24
02YK-39	Xieji, Gaozhou	mylonitic migmatite	111°00′31″ 21°55′19″	224.7 ± 0.4 (4–11)	224.5 ± 0.4	85.1	294.6	1.27
			D_3-Related Mylonites					
02YK-09	Puzhou, Yangchun	mylonitic gneiss	111°21′57″ 22°07′45″	207.8 ± 0.2 (4–12)	207.7 ± 0.3	89.1	293.3	0.66
02YK-12	Shaniutang, Yangchun	mylonitic gneiss	110°37′19″ 22°11′36″	209.0 ± 0.2 (4–11)	208.7 ± 0.3	86.7	295.6	0.71
02YK-15	Yongning, Yangchun	mylonite	111°32′39″ 22°16′49″	211.5 ± 0.5 (4–11)	209.5 ± 0.4	83.2	309.4	5.77
02YK-56	Lingwei, Bobai	granitic mylonite	109°50′24″ 21°57′54″	218.4 ± 0.3 (4–12)	218.2 ± 0.4	86.7	290.4	1.26
02YK-64	Licun, Rongxian	mylonite	110°42′00″ 22°36′11″	211.1 ± 0.2 (3–12)	211.4 ± 0.4	90.7	291.2	0.61
02YK-80	Tengbin, Luoding	mylonitic granite		208.9 ± 1.4 (3–10)	208.8 ± 1.2	94.5	298.4	2.31
02YK-26	Qianpai, Xinyi	mylonitic gneiss	111°10′33″ 22°22′31″	214.2 ± 0.4 (4–12)	215.2 ± 0.4	84.2	283.6	2.03
02YK-31	7 km north of Baishi	mylonitic granite	111°04′00″ 22°25′04″	216.9 ± 0.3 (4–12)	217.0 ± 0.4	89.3	291.9	0.89

~10°C/Ma, which is typical for most Phanerozoic orogens [e.g., *Faure et al.*, 1996; *Monir et al.*, 1994]. The $^{40}Ar/^{39}Ar$ plateau age of 230–220 Ma for D_2-related synkinematic biotites is considered as the best estimate for the minimum age of the D_2 shearing deformation within the Yunkaidashan Belt.

[31] The following data also provide important information for the timing of the D_2 deformation within the Yunkaidashan Belt. (1) Luoding thrust-and-fold sheet, as discussed above, is uncomfortably overlain by middle section of the upper Triassic sandstone and conglomerate [*Bureau of Geology and Mineral Resources of Guangdong Province*, 1988] suggesting thrusting had ceased by ~220 Ma on the basis of the timescale of *Gradstein et al.* [2004]. (2) Shiwandashan basin, a foreland basin associated with the evolution of the Yunkaidashan Belt, formed during the late Permian–middle Triassic periods (~260–230 Ma [*Liang et al.*, 2004; *Liang and Li*, 2005]). (3) Sinian to early Triassic (~245 Ma) sequences are involved in the deformation and the middle section of the upper Triassic (~220 Ma) rocks unconformably overlie the pre-Triassic strata; (4) Cordierite-bearing peraluminous granites from the Shiwandashan and western Yunkaidashan Belt, interpreted as the anatexic products during crustal thickening, have SHRIMP zircon U-Pb ages of 237–230 Ma [*Deng et al.*, 2004; *Survey Bureau of Regional Geology of Fushan*, 2004], similar to those from the other areas in the South China Block which crystallized at 243–228 Ma with a maximum frequency of ~236 Ma [*Xu et al.*, 2003; *Y. J. Wang et al.*, 2005a, 2007a, and references therein]. The Napeng granitic intrusion within the northern Yunkaidashan Belt, which is overprinted by greenschist-facies D_3 deformation yielded a SHRIMP zircon U-Pb age of 243 Ma (Survey Bureau of Regional Geology of Fushan, 2004) and is intruded by the undeformed Tengbin pluton with a LA-ICPMS zircon age of 208 ± 6 Ma [*B. X. Peng et al.*, 2006]. (5) Granulite xenolith within a charnokite pluton with the crystallization age of 212–235 Ma in the Shiwandashan area yielded a SHRIMP metamorphic zircon U-Pb age of 248 ± 6 Ma [*Peng et al.*, 2004; *Deng et al.*, 2004] and may represent maximum thickening of the crust during D_2 event. (6) The synkinematic micas from the Fengjie thrust fault yielded $^{40}Ar/^{39}Ar$ plateau ages of 247–235 Ma [e.g., *Peng et al.*, 1996]. The data, therefore, together with above-mentioned $^{40}Ar/^{39}Ar$ dating results for D_2-related synkinematic biotites suggests that the D_2 deformation was probably initiated by ~248 Ma and lasted till ~220 Ma (approximately early Triassic to earliest Late Triassic).

[32] The synkinematic D_3 biotites are from greenschist-facies mylonites. Quartz ⟨c⟩-axis fabrics are dominated by basal⟨a⟩ gliding pattern and the relevant deformation temperatures are likely in the range of 300°–400°C. This indicates the temperature of D_3 deformation is near to the argon closure temperature of synkinematic biotites. Thus the plateau ages of 218–208 Ma for these biotites are interpreted as the timing for the D_3 event (Late Triassic). This is further constrained by (1) earliest Indosinian mafic magmatism in the South China Block (Daoxian gabbro), which is related to an extensional setting, is dated at ~224 Ma [*Guo et al.*, 1997] (and Y. J. Wang's unpublished SHRIMP zircon U-Pb data, 2007); (2) Indosinian peraluminous granites from the South China Block, interpreted to form in response to magma underplating rather than crustal thickening, are dated at 220–208 Ma [e.g., *Ding et al.*, 2005; *B. X. Peng et al.*, 2006; *Y. J. Wang et al.*, 2005a, 2007a, and references therein]; (3) Late Triassic to Early Jurassic sequences uncomfortably overlying the pre-Triassic foreland molasse sediments in the Shiwandashan area are interpreted to have formed in extensional basins [*Liang et al.*, 2004; *Liang and Li*, 2005; *Bureau of Geology and Mineral Resources of Guangxi Zhuang Autonomous Region*, 1985]. Thus the D_3 event took place during the late Triassic.

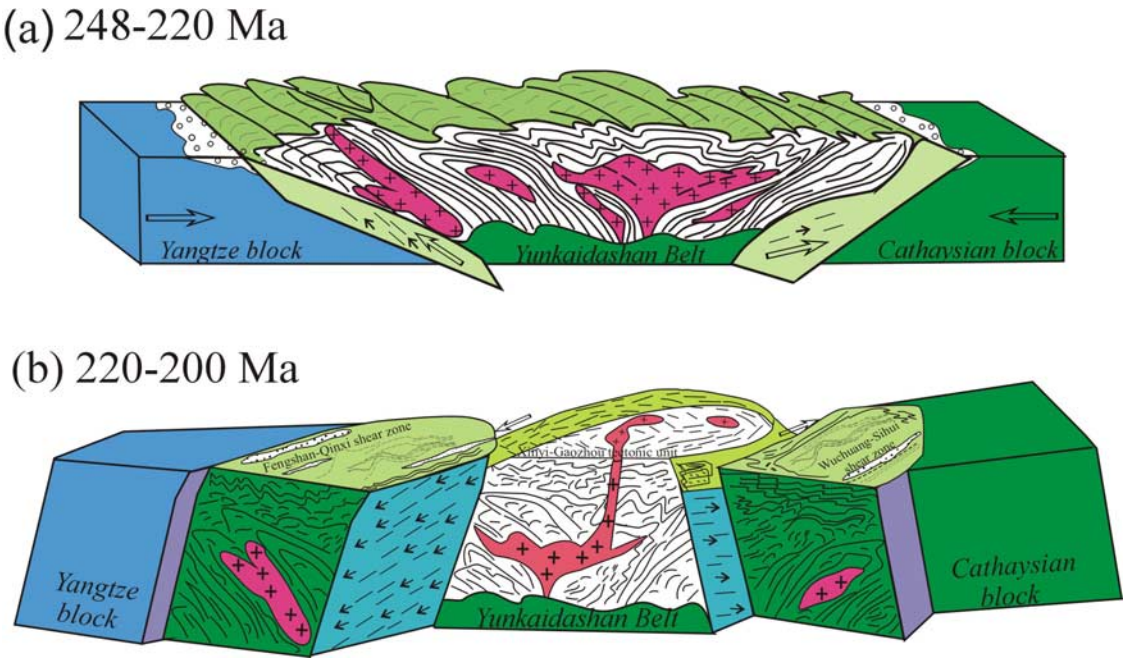

Figure 9. (a) A schematic illustration of D_2 thrusting-dominated transpression in the Yunkaidashan tectonic belt during the middle Triassic time (~248–220 Ma) in response to intracontinental oblique convergence between the Yangtze and Cathaysian blocks. (b) A schematic illustration of the Fengshan-Qinxi shear zone, Xinyi-Gaozhou tectonic unit, and Wuchuang-Sihui shear zone in the Yunkaidashan tectonic belt showing the D_3 sinistral transtensional fabrics during Late Triassic (~220–200 Ma) responsible for the collapse of the overthickened crustal segment of the Yunkaidashan belt.

6.2. Indosinian Structural Evolution of the Yunkaidashan Belt

[33] In previous studies, the Indosinian structural pattern of the Yunkaidashan Belt has been interpreted as a simple thrust sheet geometry [*Peng et al.*, 1996; *Qiu and Chen*, 1993]. However, our data document two separate phases of deformation (D_2 and D_3) responsible for the Indosinian structural evolution of the belt.

[34] D_2 structures are characterized by a series of thrust-and-fold sheets with an asymmetric thrust pattern (Figures 2, 3, and 5). The variations in S-L fabric intensity and the variable orientation of L_2 are inconsistent with those predicted by simple thrust sheet geometry and suggest a subsidiary strike-slip component during the dip-slip shortening [e.g., *Peng et al.*, 1996; *Y. J. Wang et al.*, 2005b]. Figure 9a is a schematic NW–SE cross section through the Yunkaidashan Belt during the mid-Triassic D_2 event. The cross section shows a pattern, similar to an antiformal push-up, that comprises a series of anatomizing convex-upward faults and folds, with gentle dip at the surface, which steepen progressively at depth [*Richard and Krantz*, 1991; *Ellis et al.*, 1998; *Cobbold et al.*, 2001], similar to those of the Taythes anticline [*Woodcock and Rickards*, 2003] and Teslin tectonic zone [*Stevens and Erdmer*, 1996]. Such a pattern indicates a positive flower-like or palm-tree structure associated with transpression at the regional scale.

[35] Synthesis of all the structural observations (Figures 1–5) most likely points to a thrust-type sinistral transpression in the Yunkaidashan Belt during D_2 event in which crustal segments of the Yangtze and Cathaysian blocks (west and east of the Yunkaidashan belt, respectively) are obliquely underthrust beneath the belt (Figure 9a). The continuously oblique thrusting of the crustal segments resulted in significant crustal thickening and upward extrusion, and then the development of a flower-like structural pattern. The spatial distribution of Indosinian metamorphism, granulitic xenoliths, charnockites and peraluminous granites [e.g., *Bureau of Geology and Mineral Resources of Guangdong Province*, 1988; *Bureau of Geology and Mineral Resources of Guangxi Zhuang Autonomous Region*, 1985; *Peng et al.*, 2004; *Deng et al.*, 2004], suggests the western Yunkaidashan belt underwent greater tectonic thickening than the eastern Yunkaidashan belt and thus it is very likely that the Yangtze block was underthrust to depths of >50 km.

[36] Ultimately the overthickened crustal segment of the overriding unit (the Yunkaidashan Belt) would need to isostatically re-adjust owing to the increased buoyancy of the downgoing segment [*Thompson et al.*, 2001; *Konopásek et al.*, 2005], resulting in collapse of the belt and development of the transtensional shear zones. As a result, the regime of the D_2 oblique thrusting changed into D_3 sinistral transtensional movement. During the D_3 transtensional movement, the Xinyi-Gaozhou tectonic unit lay in the

footwall to the Fengshan-Qinxi and Wuchuang-Sihui shear zones (Figure 9b). Most D_3 deformation was of sinistral strike-slip character under greenschist-facies condition, and predominantly concentrated in the Wuchuang-Sihui and Fengshan-Qinxi areas (Figures 1c, 2, and 3). For example, in the Wuchuang-Sihui shear zone, the D_3 deformation resulted in almost complete transposition of the D_2 fabric. In contrast, the intensity of the D_3 overprinting decreased significantly in the Xinyi-Gaozhou block where the D_3 fabric is dominated by refolding of D_2 structural elements, newly developed F_3 foliation and small-scale D_3 shear zone. These structural and regional relations, in combination with above-mentioned biotite $^{40}Ar/^{39}Ar$ age data, suggest a two-stage evolution for the Indosinian orogeny of the Yunkaidashan Belt: thrusting- dominated D_2 sinistral transpression in the early middle Triassic (~248–220 Ma) followed by D_3 sinistral transtension in the late Triassic (~220–200 Ma).

6.3. Indosinian Pattern of the South China Block

[37] Structural patterns from regions adjoining the Yunkaidashan Belt (Xuefengshan, Wugongshan and Wuyishan as shown in Figure 1b) help constrain the overall character of Indosinian orogenesis in the South China Block. To the west of the Yunkaidashan belt, the Xuefengshan tectonic zone is characterized by top-to-WNW-thrusting and top-to-ESE-back thrusting with a sinistral strike-slip component during the middle Triassic to early Jurassic (244–195 Ma [*Y. J. Wang et al.*, 2005b]). A well-developed Mesozoic thrust system with both thin- and thick-skinned thrusts extends through the Xuefengshan to the Sichuan basin (from SE to NW [*Yan et al.*, 2003]). To the east of Yunkaidashan Belt, southeast-verging thrusting appears to dominate in the Wuyishan belt during the early and middle Triassic on the basis of the detailed field mapping in western Fujian province [*Chen*, 1999; *Chen et al.*, 1998; *Zhu et al.*, 1997] (and Y. J. Wang's unpublished data, 2007). These data, in combination with the D_2 pattern of the Yunkaidashan Belt, reveal a large-scale, early Indosinian positive flower-like structural pattern from Xuefengshan (western flank) to Yunkaidashan (center), and onto Wuyishan (eastern flank). The east-west geoscience transect across the South China Block also shows an overall mirror-image thrusting geometry with the zone of crustal thickening corresponding with the core of the proposed flower structure [*Yuan et al.*, 1989; *Chen*, 1999, Figure 13].

[38] Late Triassic D_3 transtensional structures from regions adjoining the Yunkaidashan belt are focused along zones of D_2 compression. For example, in the Wugongshan dome divergent noncoaxial extension during late Triassic [e.g., *Faure et al.*, 1996] follows an earlier phase of compressive deformation [*Wang et al.*, 2001] (and Y. J. Wang et al.'s unpublished data, 2007). Similarly an extensional tectonic phase immediately follows compression in the Jiulingshan zone and Lushan dome during middle-late Triassic times [*Lin et al.*, 2001]. Thus Indosinian orogenesis in the South China Block shows a succession of events involving early middle Triassic thrusting-related transpression and development of a large-scale flower structure [e.g., *Chen*, 1999; *Y. J. Wang et al.*, 2005b] that developed in a regime of oblique regional convergence, and subsequent late Triassic transtension within the overthickened gravitationally unstable crustal segment.

6.4. Implications on the Indosinian Tectonics of the South China Block

[39] Driving mechanisms that have been invoked for Indosinian orogenesis in South China involve either oceanic/arc-continental subduction/collision [*Holloway*, 1982; *Hsü et al.*, 1990; *Li*, 1998; *Li et al.*, 2006; *Zhou and Li*, 2000] or intracontinental collision [*Zhou and Li*, 2000; *Chen*, 1999; *Xu et al.*, 1993; *Y. J. Wang et al.*, 2005a]. Recently, *Li and Li* [2007] have attempted to integrate the subduction and intracontinental collision hypotheses by invoking a flat-slab subduction model of the paleo-Pacific plate to explain deformation and granite magmatism up to 1300 km from the inferred subduction zone. However, we consider that a number of potential problems with this model argue against its validity in explaining Indosinian orogenesis. The westward subduction of the Pacific plate may not have initiated until ~125 Ma (mid-Early Cretaceous [*Engebretson et al.*, 1985; *Metcalfe*, 1996, 2002; *Veevers*, 2004]). Also, late Paleozoic to early Mesozoic arc magmatism is not recognized in the South China Block. According to the *Li and Li*'s [2007] model, SE-dipping thrusting, synorogenic magmatism and foreland basin deposition should propagate toward the cratonic interior in response to developing flat slab subduction of Pacific Ocean lithosphere. However, our observations demonstrate that the D_2 structural pattern is a huge flower structure [e.g., *Faure et al.*, 1996; *Chen*, 1999; *Y. J. Wang et al.*, 2005b] with NW directed thrusting in the west and SE directed thrusting in the east, rather than a migrating, top-to-the-NW fold and thrust belt [e.g., *Faure et al.*, 1996; *Chen*, 1999; *Yan et al.*, 2003; *Zhu et al.*, 1997; *Y. J. Wang et al.*, 2005b, and references therein]. Foreland basin development is spatially and temporally restricted with the Youjiang-Shiwandashan Basin lying to just west of the Yunkaidashan belt and only developed during the latest Permian to middle Triassic (~260–235 Ma). Age data on magmatic activity does not young to the NW as suggested by *Li and Li* [2007] but appears to consist of two spatially overlapping belts of activity with ages of 246–228 Ma and 220–208 Ma [*Y. J. Wang et al.*, 2005a, 2007a, and references therein].

[40] Early Mesozoic Indosinian orogenesis overlaps with the final stages of Pangea assembly and resultant global kinematic readjustments [*Cawood and Buchan*, 2007]. In particular this timeframe corresponds with opening of the Tethys Ocean and breaking off from the northern Gondwana segment of the supercontinent of a series of microcontinental ribbons and their resultant drift across the Tethys and accretion to Asia [*Veevers*, 2000, 2004; *Cawood*, 2005; *Cawood et al.*, 2007; *Metcalfe*, 1996, 2002]. This drove subduction and collision along the southern and northern margins of the South China Block (Figure 10a). The northern margin of the block was deeply subducted northward beneath the North China Block during early Triassic, resulting in the Dabie-Sulu Orogeny [e.g., *Li et al.*, 1993;

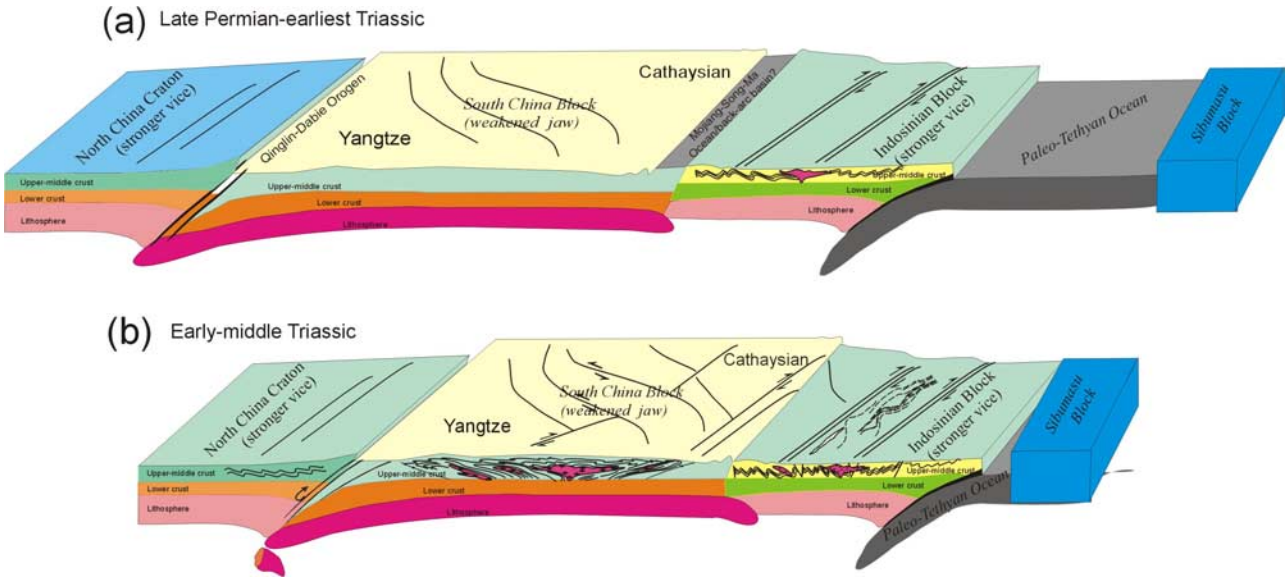

Figure 10. A schematic cartoon showing (a) Late Permian–earliest Triassic tectonic pattern of the North China Craton, South China Block, and Indosinian Blocks accompanied with the closure of the Paleo-Tethyan Ocean and (b) early middle Triassic intracontinental convergence of the South China Block in response to the collision of the Sibumasu and Indosinian blocks. The South China Block acts as a hot, wide and less competent orogen whereas the North China and Indosinian Blocks act as the stronger and more competent blocks.

Hacker et al., 1998]. At the southern margin, the paleo-Tethys Ocean closed and the Sibumasu Block collided with the Indosinian Block during late Permian-middle Triassic [e.g., *Carter et al.*, 2001; *Metcalfe*, 1996, 2002; *Lepvrier et al.*, 2004; *Zhong*, 1998; *S. B. Peng et al.*, 2006]. This subduction/collision history is spatially and temporally coupled with early Indosinian transpression in the South China Block.

[41] Figure 10 is a schematic Triassic regional cross section orientated approximately north-south and running from the North China Block across the South China and Indosinian blocks to the subducting Tethys Ocean and the soon to be accreted Sibumasu Block. The pre-Triassic crustal architecture of the South China Block includes extensive magmatic activity built up from Neoproterozoic–early Paleozoic rifting following the break-up of Rodinia and strong Caledonian and Indosinian tectonomagmatic pulses [e.g., *Liu*, 1991; *Hunan Bureau of Geology and Mineral Resources*, 1988; *Bureau of Geology and Mineral Resources of Guangdong Province*, 1988; *Goodel et al.*, 1991; *Wang and Li*, 2003]. Triassic anatexic granites are spatially compatible with the Indosinian flower structure, suggestive of a hot and partially melted middle-lower crust during the Triassic [*Y. J. Wang et al.*, 2005b, 2007a, 2007b, and references therein]. Thus the South China Block was a relatively weak, wide and buoyant region during Indosinian orogenesis that lay between the more rigid North China and Indosinian blocks. We propose that the closure of Paleo-Tethyan Ocean and subsequent collision of the Indosinian with South China Blocks and the Sibumasu with Indosinian Blocks during the assembly of Pangea drove Triassic South China intracontinental orogenesis and resulted in development of a broad, crustal-scale positive flower structure (Figure 10). Analogue and numerical experiments have documented similar behavior and crustal architecture for weakened blocks squeezed within a vice of stronger blocks [e.g., *Cobbold et al.*, 2001; *Ellis et al.*, 1998; *Willett et al.*, 1993; *Cruden et al.*, 2006].

[42] **Acknowledgments.** We thank Y.-H. Zhang for helpful discussions and suggestions. We also thank Henri Maluski and an anonymous reviewer for their thorough, critical, and constructive reviews and comments, and Onno Oncken for his helpful editorial advice. This study was jointly supported by grants from the Natural Science Foundation of China (40772129 and 40421303) and Chinese Academy of Sciences (kzcx2-yw-128). This is Tectonics Special Research Centre Publication 413 and is a contribution to International Lithosphere Program ERAS (EaRth Accretionary Systems in space and time).

References

Bureau of Geology and Mineral Resources of Guangdong Province (GDBGMR) (1988), *Regional Geology of Guangdong Province* (in Chinese), pp. 1–602, Geol. Publ. House, Beijing.

Bureau of Geology and Mineral Resources of Guangxi Zhuang Autonomous Region (GXBGMR) (1985), *Regional Geology of the Guangxi Autonomous Region* (in Chinese), pp. 1–853, Geol. Publ. House, Beijing.

Bureau of Geology and Mineral Resources of Jiangxi Province (JXBGMR) (1984), *Regional Geology of the Jiangxi Province* (in Chinese), pp. 1–921, Geol. Publ. House, Beijing.

Cai, M. H., M. G. Zhan, and S. B. Peng (2001), Study of Mesozoic metallogenic geological setting and dynamic mechanism in Yunkai area (in Chinese), *Miner. Deposits*, *21*(3), 264–269.

Carter, A., D. Roques, and C. Bristow (2001), Understanding Mesozoic accretion in southeast Asia: Significance of Triassic thermotectonism (Indosinian orogen) in Vietnam, *Geology*, *29*(3), 211–214.

Cawood, P. A. (2005), Terra Australis Orogen: Rodinia breakup and development of the Pacific and Iapetus margins of Gondwana during the Neoproterozoic and Paleozoic, *Earth Sci. Rev.*, *69*, 249–279.

Cawood, P. A., and C. Buchan (2007), Linking accretionary orogenesis within supercontinental assembly, *Earth Sci. Rev.*, *82*, 217–256.

Cawood, P. A., M. R. W. Johnson, and A. A. Nemchin (2007), Early Paleozoic orogenesis along the India margin of Gondwana: Tectonic response to Gondwana assembly, *Earth Planet. Sci. Lett.*, *255*, 70–84.

Chen, A. (1999), Mirror thrusting in the south China orogenic belt: Tectonic evidence from western Fujian, southeastern China, *Tectonophysics*, *305*, 497–519.

Chen, B., and Y. X. Zhuang (1994), The petrology and petrogenesis of Yunlu chamockite and its granite inclusion, western Guangdong, South China (in Chinese), *Acta Pet. Sin.*, *10*(2), 139–150.

Chen, D. F., X. H. Li, J. M. Pang, W. Q. Dong, G. Q. Chen, and X. P. Chen (1998), Metamorphic newly produced zircon, SHRIMP ion microprobe U-Pb age of amphibolite of Hexi Group, Zhejiang and its implication, *Acta Miner. Sin.*, *18*(4), 396–400.

Chen, J. F., and B. M. Jahn (1998), Crustal evolution of southeastern China: Nd and Sr isotopic evidence, *Tectonophysics*, *284*, 101–133.

Cobbold, P. R., S. Durand, and R. Mourgues (2001), Sandbox modeling of thrust wedges with fluid- assisted detachments, *Tectonophysics*, *334*, 245–258.

Cruden, A. R., M. H. B. Nasseri, and R. Pysklywec (2006), Surface topography and internal strain variation in wide hot orogens from three-dimensional analogue and two-dimensional numerical vice models, in *Analogue and Numerical Modeling of Crustal-Scale Process*, edited by S. J. H. Buiter and G. Schreurs, *Geol. Soc. Spec. Publ.*, *253*, 79–104.

Deng, X. G., Z. G. Chen, and X. H. Li (2004), SHRIMP U-Pb zircon dating of the Darongshan-Shiwandashan (in Chinese with English abstract), *Geol. Rev.*, *50*(4), 426–432.

Deprat, J. (1914), Etude des plissements et des zones décrasement de la moyenne et de la basse Rivière Noire, *Mem. Serv. Geol. Indochine*, *3*, 59.

Ding, X., P. R. Chen, W. F. Chen, H. Y. Huang, and X. M. Zhou (2005), LA-ICPMS zircon dating of Weishan granitic plutons in Hunan Province: Petrogenesis and tectonic implications, *Sci. China, Ser. D*, *35*(7), 606–616.

Dodson, M. H. (1973), Closure temperature in cooling geochronological and petrological systems, *Contrib. Miner. Petrol.*, *40*, 259–274.

Ellis, S., B. Beaumont, R. A. Jamieson, and G. Quinlan (1998), Continental collision including a weak zone: The vise model and its application to the Newfoundland Appalachians, *Can. J. Earth. Sci.*, *35*, 1323–1346.

Engebretson, D. C., A. Cox, and R. G. Gordon (1985), Relative motions between oceanic and continental plates in the Pacific basins, *Spec. Pap. Geol. Soc. Am.*, *206*, 1–59.

Faure, M., Y. Sun, L. Shu, P. Monié, and J. Charvet (1996), Extensional tectonics within a subduction-type orogen: The case study of the Wugongshan dome (Jiangxi Province, southeastern China), *Tectonophysics*, *263*, 77–106.

Fromaget, J. (1932), Sur la structure des Indosinides, *C. R. Hebd. Seances Acad. Sci.*, *195*, 538.

Goodel, P. C., S. Gilder, and X. Fang (1991), A preliminary description of the Gan-Hang failed rift, southeastern China, *Tectonophysics*, *197*, 245–255.

Gradstein, F. M., J. G. Ogg, and A. G. Smith (2004), *A Geologic Time Scale 2004*, 589 pp., Cambridge Univ. Press, New York.

Guo, F., W. M. Fan, and G. Lin (1997), Sm-Nd dating and pegrogenesis of Mesozoic gabbro xenolith in Daoxian County, Hunan Province, *Chin. Sci. Bull.*, *42*(17), 1661–1663.

Hacker, B. R., L. W. Ratschbacher, and L. Ireland (1998), U/Pb zircon ages constrain the architecture of the ultrahigh-pressure Qinling-Dabie Orogen, China, *Earth Planet. Sci. Lett.*, *161*, 215–230.

Hames, W. E., and S. A. Bowring (1995), An empirical evaluation of the argon diffusion geometry in muscovite, *Earth Planet. Sci. Lett.*, *124*, 161–167.

Harrison, T. M., I. Duncan, and L. McDougall (1985), Diffusion of ^{40}Ar in biotite: temperature, pressure and compositional effects, *Geochim. Cosmochim. Acta*, *49*, 2461–2468.

Hodges, K. V., W. E. Hames, W. Olszewski, B. C. Burchfiel, L. H. Royden, and Z. Chen (1994), Thermobarometric and ^{40}Ar/^{39}Ar geochronological constraints on Himalayan metamorphism in the Dinggye area, southern Tibet, *Contrib. Mineral. Petrol.*, *117*(2), 151–163.

Holloway, N. H. (1982), North Palawan Block, Philippines: Its relation to Asian mainland and role in evolution of South China Sea, *Am. Assoc. Pet. Geol. Bull.*, *66*, 1355–1383.

Hsû, K. J., J. L. Li, H. H. Chen, Q. C. Wang, S. Sun, and A. M. Y. Sengör (1990), Tectonics of South China: Key to understanding west Pacific geology, *Tectonophysics*, *193*, 9–39.

Huang, J. Q., J. S. Ren, C. F. Jiang, Z. K. Zhang, and D. Y. Qin (1987), *Geotectonic Evolution of China*, pp. 1–203, Springer, Berlin.

Hunan Bureau of Geology and Mineral Resources (HNBGMR) (1988), *Regional Geology of the Hunan Province* (in Chinese), pp. 286–507, Geol. Publ. House, Beijing.

Konopásek, J., S. Kroner, S. L. Kitt, C. W. Passchier, and A. Kröner (2005), Oblique collision and evolution of large-scale transcurrent shear zones in the Kaoko belt, NW Namibia, *Precambrian Res.*, *136*(2), 139–157.

Law, R. O. (1990), Crystallographic fabrics: A selective review of their applications to research in structural geology, in *Deformation Mechanism, Rheology and Tectonics*, edited by R. J. Knipe and E. H. Rutter, *Geol. Soc. Spec. Publ.*, *54*, 335–352.

Lepvrier, C., H. Maluski, V. V. Tich, A. Leyerloup, T. P. Truong, and V. V. Nguyen (2004), The Early Triassic Indosinian orogeny in Vietnam (Truong Son Belt and Kontum Massif): Implications for the geodynamic evolution of Indochina, *Tectonophysics*, *393*, 87–118.

Li, S. G., Y. Chen, B. L. Cong, Z. Zhang, Y. Zhang, D. L. Liou, S. A. Hart, and N. Ge (1993), Collision of the North China and Yangtze Blocks and formation of coesite-bearing eclogites: Timing and processes, *Chem. Geol.*, *109*, 80–89.

Li, X. H., Z. X. Li, W. X. Li, and Y. J. Wang (2006), Initiation of the Indosinian Orogeny in South China: Evidence for a Permian magmatic arc in the Hainan Island, *J. Geol.*, *114*(3), 341–353.

Li, Z. X. (1998), Tectonic history of the major East Asian lithospheric blocks since the mid-Proterozoic: A synthesis, in *Mantle Dynamics and Plate Interactions in East Asia*, *Geodyn. Ser.*, vol. 27, edited by M. F. J. Flower et al., pp. 221–243, AGU, Washington, D. C.

Li, Z. X., and X. H. Li (2007), Formation of the 1300-km-wide intracontinental orogen and postorogenic magmatic province in Mesozoic south China: A flat-slab subduction model, *Geology*, *35*(2), 179–182.

Liang, X. Q., and X. H. Li (2005), Late Permian to Middle Triassic sedimentary records in Shiwandashan Basin: Implication for the Indosinian Yunkai orogenic Belt, south China, *Sediment. Geol.*, *177*, 297–320.

Liang, X. Q., X. H. Li, and Y. X. Qiu (2004), Intracontinental collisional orogeny during Late Permian-Middle Triassic in south China: Sedimentary records of the Shiwandashan Basin, *Acta Geol. Sin.*, *78*, 756–762.

Lin, W., M. Faure, Y. Sun, L. S. Shu, and Q. C. Wang (2001), Compression to extension switch during the Middle Triassic orogeny of eastern China: The case study of the Jiulingshan massif in the southern foreland of the Dabieshan, *J. Earth Sci.*, *20*(1), 31–43.

Liu, H. Y. (1991), Correlation of the Sinian System, in *The Sinian System in China* (in Chinese), edited by H. Liu, pp. 126–170, Science Press, Beijing.

Lo, C. H., T. C. Onstott, C. H. Chen, and T. Lee (1994), An assessment of ^{40}Ar/^{39}Ar dating for the whole-rock volcanic samples from the Luzon arc near Taiwan, *Chem. Geol.*, *114*, 157–178.

Metcalfe, I. (1996), Pre-Cretaceous evolution of SE Asian terranes, in *Tectonic Evolution of Southeast Asia*, edited by R. Hall and D. Blundell, *Geol. Soc. Spec. Publ.*, *106*, 97–122.

Metcalfe, I. (2002), Permian tectonic framework and palaeogeography of SE Asia, *J. Asian Earth Sci.*, *18*, 691–712.

Monir, P., R. L. Torres-Roldan, and A. Garcia-Casco (1994), Cooling and exhumation of the Western Betic Cordilleras, ^{40}Ar/^{39}Ar thermochronological constraints on a collapsed terrane, *Tectonophysics*, *238*, 353–379.

Peng, B. X., Y. J. Wang, W. M. Fan, T. P. Peng, and X. Q. Liang (2006), LA-ICPMS zircon U-Pb dating for three typical granitic plutons from Central Hunan and western Guangdong Provinces and its petrogenetic implications, *Acta Geol. Sin.*, *80*, 660–669.

Peng, S. B., J. Y. Fu, and Y. H. Lou (2004), The discovery and significance of A-type charnokite in southeast Guangxi Province, *Sci. Technol. Eng.*, *4*(10), 832–834.

Peng, S. B., Z. M. Jin, J. M. Fu, Y. H. Liu, L. Q. He, M. H. Cai, and Y. B. Wang (2006), The petrochemistry, geochronology and gnesiso banded-augen strong peraluminous granitoids in Yunkai orogenic belt, western Guangdong Province (in Chinese), *China Earth Sci.*, *37*(1), 110–120.

Peng, S. M., L. F. Fu, and G. Q. Zhou (1996), *Tectonic Evolution of Yunkai Massif and Its Shearing Anatectic Origin of Gneissic Granitic Rocks*, 167 pp., China Univ. Geosci. Press, Beijing.

Purdy, J. W., and E. Jäger (1976), K-Ar ages on rock-forming minerals from the Central Alps, *Mem. Inst. Geol. Mineral.*, *30*, 1–31.

Qiu, Y. X., and H. J. Chen (1993), *Procession of Geological Structure of Yunkaidashan and Its Adjacent Areas* (in Chinese), pp. 1–74, Geol. Publ. House, Beijing.

Ren, J. S. (1991), On the geotectonics of southern China, *Acta Geol. Sin.*, *2*, 111–136.

Richard, P., and R. W. Krantz (1991), Experiments on fault reactivation in strike-slip mode, *Tectonophysics*, *188*, 113–117.

Sang, H. Q., S. S. Wang, and J. Qiu (1996), The ^{40}Ar/^{39}Ar ages of pyroxene, hornblende and plagioclase in Taipingzhai granulites in Qianxi County, Hebei Province and their geological implications (in Chinese), *Acta Petrol. Sin.*, *12*(4), 390–400.

Stevens, R. A., and P. Erdmer (1996), Structural divergence and transpression in the Teslin tectonic zone, southern Yukon Territory, *Tectonics*, *15*(6), 1342–1363.

Survey Bureau of Regional Geology of Fushan (FSSBRG) (2004), Geological map of the Yangchun, Guangdong Province (in Chinese), map, 1:250000 scale, Guangzhou, China.

Thompson, A. B., K. Schulmann, J. Jezek, and V. Tolar (2001), Thermally softened continental extensional zones (arcs and rifts) as precursors to thickened orogenic belts, *Tectonophysics*, *332*, 115–141.

Tullis, J., J. M. Christie, and D. T. Griggs (1973), Microstructure and preferred orientations of experimentally deformed quartzites, *Geol. Soc. Am. Bull.*, *84*, 297–314.

Twiss, R. J., and E. M. Moores (1994), *Structural Geology*, pp. 215–422, W. H. Freeman, New York.

Veevers, J. J. (2000), *Billion-Year Earth History of Australia and Neighbours in Gondwanaland*, 388 pp., GEMOC Press, Sydney.

Veevers, J. J. (2004), Gondwanaland from 650–500 Ma assembly through 320 Ma merge in Pangea to 185–100 Ma breakup: Supercontinental tectonics via stratigraphy and radiometric dating, *Earth Sci. Rev.*, *68*, 1–132.

Wang, D. Z., L. S. Shu, M. Faure, and W. Z. Shen (2001), Mesozoic magmatism and granitic dome in the Wugongshan Massif, Jiangxi province and their genetic relationship to the tectonic events in southeast China, *Tectonophysics*, *339*, 259–277.

Wang, J., and Z. X. Li (2003), History of Neoproterozoic rift basins in south China: Implications for Rodinia break-up, *Precambrian Res.*, *122*(1–4), 141–158.

Wang, J. H., X. L. Tu, and D. Z. Sun (1999), U-Pb dating of anatectic migmatites at Gaozhou in the Yunkai block, western Guangdong, China (in Chinese with English abstract, *Geochimica*, *28*(3), 231–238.

Wang, Q., J. W. Li, P. Jian, Z. H. Zhao, X. L. Xiong, Z. W. Bao, J. F. Xu, C. F. Li, and J. L. Ma (2005), Alkaline syenites in eastern Cathaysia (south China): Link to Permian-Triassic transtension, *Earth Planet. Sci. Lett.*, *230*, 339–354.

Wang, Y. J., W. M. Fan, X. Q. Liang, T. P. Peng, and Y. R. Shi (2005a), SHRIMP zircon U-Pb geochronology of Indosinian granites in Hunan Province and its petrogenetic implications, *Chin. Sci. Bull.*, *50*(13), 1395–1403.

Wang, Y. J., Y. H. Zhang, W. M. Fan, and T. P. Peng (2005b), Structural signatures and $^{40}Ar/^{39}Ar$ geochronology of the Indosinian Xuefengshan transpressive belt, south China interior, *J. Struct. Geol.*, *27*, 985–998.

Wang, Y. J., W. M. Fan, M. Sun, X. Q. Liang, Y. H. Zhang, and T. P. Peng (2007a), Geochronological, geochemical and geothermal constraints on petrogenesis of the Indosinian peraluminous granites in the South China Block: A case study in the Hunan Province, *Lithos*, *96*, 475–502.

Wang, Y. J., W. M. Fan, G. C. Zhao, S. C. Ji, and T. P. Peng (2007b), Zircon U-Pb geochronology of gneisses in Yunkai Mountains and its implications on the Caledonian event in the South China, *Gondwana Res.*, *12*(4), 404–416.

Willett, S., C. Beaumont, and P. Fullsack (1993), A mechanical model for the tectonics of doubly vergent compressional orogens, *Geology*, *21*, 371–374.

Woodcock, N. H., and B. Rickards (2003), Transpressive duplex and flower structure: Dent Fault System, NW England, *J. Struct. Geol.*, *25*, 1981–1992.

Xu, J. W., G. Ma, W. X. Tong, G. Zhu, and S. Lin (1993), Displacement of the Tancheng-Lujiang wrench fault system and its geodynamic setting in the northwestern Circum-Pacific, in *The Tanchang-Lujiang Wrench Fault System*, edited by J. Xu, pp. 51–74, John Wiley, Hoboken, N. J.

Xu, X. S., P. Deng, and S. Y. O'Reilly (2003), Single zircon LAM ICPMS U-Pb dating of Guidong complex (SE China) and its petrogenetic significance, *Chin. Sci. Bull.*, *48*(17), 1892–1899.

Xu, X. S., S. Y. O'Reilly, W. L. Griffin, P. Deng, and N. J. Pearson (2005), Relict Proterozoic basement in the Nanling Mountains (SE China) and its tectonothermal overprinting, *Tectonics*, *24*(2), TC2003, doi:10.1029/2004TC001652.

Yan, D. P., M. F. Zhou, H. L. Song, X. W. Wang, and J. Malpas (2003), Origin and tectonic significance of a Mesozoic multi-layer over-thrust system within the Yangtze bock (South China), *Tectonophysics*, *361*, 239–254.

Yardley, B. W. D. (1989), *An Introduction to Metamorphic Petrology*, Longman, London.

Yuan, X. C., Y. Zuo, X. L. Cai, and J. S. Zhu (1989), The structure of the lithosphere and the geophysics in the South China Plate, in *Progress on Geophysics in China in the 1980s*, pp. 243–249, Ed. Board of Bull. of Geophys., Beijing.

Zhang, B. Y., and H. N. Yu (1994), *On the Deep-Level Nappe Structure in Hercynian-Indosinian Collision Belt in Western Guangdong* (in Chinese), 121 pp., Geol. Publ. House, Beijing.

Zhong, D. L. (1998), *Paleotethyan Orogenic Belts in Yunnan and Western Sichuan*, 230 pp., Science Press, Beijing.

Zhong, Z. Q., Z. D. You, and H. W. Zhou (1989), The evolution and basic structural framework of the basement of the Yunkai uplift (in Chinese), *Reg. Geol. China*, *15*(1), 36–43.

Zhou, H. W., Z. D. You, and Z. Q. Zhong (1994), New findings of low pressure granulite facies metamorphic age in Yunkai uplift (in Chinese), *Geol. Sci. Tech. Inform.*, *13*(3), 23–26.

Zhou, X. M., and W. X. Li (2000), Origin of Late Mesozoic igneous rocks in southeastern China: Implications for lithosphere subduction and underplating of mafic magmas, *Tectonophysics*, *326*, 269–287.

Zhu, B. Q., Y. X. Wang, H. F. Wang, D. G. Chen, and D. F. Chen (1997), Huangshan- Wenzhou geochemical section and its corridor area of lithosphere in southeast China (in Chinese with English abstract), *Geochemica*, *26*(2), 1–13.

P. A. Cawood, Tectonics Special Research Centre, University of Western Australia, Crawley WA 6009, Australia.

X. Chen, W. Fan, S. Ji, T. Peng, and Y. Wang, Key Laboratory of Isotope Geochronology and Geochemistry, Guangzhou Institute of Geochemistry, Chinese Academy of Sciences, P.O. Box 1131, Guangzhou 510640, China. (yjwang@gig.ac.cn)